Review

A Review on the Removal of Carbamazepine from Aqueous Solution by Using Activated Carbon and Biochar

María Alejandra Décima *[ID], Simone Marzeddu [ID], Margherita Barchiesi [ID], Camilla Di Marcantonio [ID], Agostina Chiavola and Maria Rosaria Boni [ID]

Department of Civil, Constructional and Environmental Engineering (DICEA), Faculty of Civil and Industrial Engineering, Sapienza University of Rome, Via Eudossiana 18, 00184 Rome, Italy; simone.marzeddu@uniroma1.it (S.M.); margherita.barchiesi@uniroma1.it (M.B.); camilla.dimarcantonio@uniroma1.it (C.D.M.); agostina.chiavola@uniroma1.it (A.C.); mariarosaria.boni@uniroma1.it (M.R.B.)
* Correspondence: mariaalejandra.decima@uniroma1.it; Tel.: +39-06-4458-5514

Abstract: Carbamazepine (CBZ), one of the most used pharmaceuticals worldwide and a Contaminant of Emerging Concern, represents a potential risk for the environment and human health. Wastewater treatment plants (WWTPs) are a significant source of CBZ to the environment, polluting the whole water cycle. In this review, the CBZ presence and fate in the urban water cycle are addressed, with a focus on adsorption as a possible solution for its removal. Specifically, the scientific literature on CBZ removal by activated carbon and its possible substitute Biochar, is comprehensively scanned and summed up, in view of increasing the circularity in water treatments. CBZ adsorption onto activated carbon and biochar is analyzed considering several aspects, such as physicochemical characteristics of the adsorbents, operational conditions of the adsorption processes and adsorption kinetics and isotherms models. WWTPs usually show almost no removal of CBZ (even negative), whereas removal is witnessed in drinking water treatment plants through advanced treatments (even >90%). Among these, adsorption is considered one of the preferable methods, being economical and easier to operate. Adsorption capacity of CBZ is influenced by the characteristics of the adsorbent precursors, pyrolysis temperature and modification or activation processes. Among operational conditions, pH shows low influence on the process, as CBZ has no charge in most pH ranges. Differently, increasing temperature and rotational speed favor the adsorption of CBZ. The presence of other micro-contaminants and organic matter decreases the CBZ adsorption due to competition effects. These results, however, concern mainly laboratory-scale studies, hence, full-scale investigations are recommended to take into account the complexity of the real conditions.

Keywords: activated carbon; adsorption; biochar; carbamazepine; charcoal; isotherms; kinetics; water treatment plants; wastewater treatment plants

1. Introduction

The presence of pharmaceuticals in environmental matrices increased consistently during the last 20 years, also due to the population grows and ages [1]. The pathway of these contaminants starts with human or veterinary consumption and metabolization, then between 30% and 90% of the dose is generally excreted as active substances through urine and feces [2]. Thus, they enter in the sewage network and arrive at the inlet of wastewater treatment plants (WWTPs). There pharmaceuticals are not completely removed, since WWTPs are not designed and operated to accomplish this aim, therefore residual concentrations can reach different environmental matrices with the effluents or wasted sludges. Furthermore, veterinary pharmaceuticals used for livestock and aquaculture can be directly released in water bodies [3]. The environmental issue is particularly challenging because pharmaceuticals are designed to interact with living organisms and to produce a response at low doses, which make them of high concern even at low concentrations. Moreover, they

are also designed to be stable and to interact only with target molecules, entailing that they are very slow to degrade. This is why their constant use leads to a continuous release and accumulation into the environment. Among pharmaceuticals, carbamazepine (CBZ) is one of the most used worldwide [4]. It is well known as a refractory molecule to traditional water and wastewater treatment processes and particularly to biological processes [3,5–7]. Additionally, CBZ exposure has harmful effects on aquatic and terrestrial organisms, such as reproduction toxicity, developmental delay and carcinogenicity [8]. For these reasons, CBZ represents a contaminant of concern for the environment and human health [9,10]; it was also proposed as a possible anthropogenic marker in waters [4].

In the literature, different technologies for CBZ removal from contaminated water are reported [4,11–13]. These technologies are mainly based on electrochemical oxidation [14,15], solar photolysis [16,17], photocatalysis [18–20], osmotic membrane separation [12,21], ion exchange [22,23], persulfate oxidation [24], ultrasound/persulfate anions oxidation [25], dielectric barrier discharge process [26,27] and ozone/ultraviolet/hydrogen peroxide advanced oxidation [28,29]. Among them, adsorption is the most used technology for its high efficiency and lower operating costs [30–32]; the first quantitative experiments about this technology involved the study of gas adsorption on charcoal (which was later called "activated carbon") and clay [33].

Many studies have investigated different adsorbents materials for CBZ removal from waters, such as activated carbon [34], silica-based materials [35] chitosan-based materials [36], granular carbon nanotubes/alumina hybrid [37] and zeolites [38]. Many of these adsorbents generally provide a high level of adsorption capacity of CBZ [39].
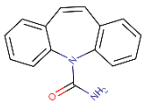
A new and sustainable adsorbent for removal of recalcitrant contaminant such as CBZ is biochar which has been already demonstrated to be a valid alternative to commercial media for the removal of various emerging micropollutants from waters [40–43]. Thus, the present review provides a comprehensive analysis of the application of biochar to CBZ removal from water and wastewater, compared to the traditional activated carbon. Specifically, the aims of this work were: (1) to discuss CBZ presence in wastewater and water treatment plants and (2) to review the adsorption process onto activated carbon and biochar considering the different factors that can influence the adsorption capacity, such as physicochemical properties and operational conditions. Finally, adsorption kinetic and isotherm models that are mostly applied to represent the experimental data of CBZ removal onto activated carbon and biochar were also discussed.

Several reviews describe the adsorption process of pharmaceuticals from water onto many types of adsorbents, however, to the best of our knowledge, this is the first review focusing on the comparison of CBZ adsorption onto activated carbon and biochar. Moreover, the information collected and discussed about the effects of operative parameters related to the adsorption process can be of great interest also for water and wastewater treatment plants managers, representing an additional novelty of the study.

2. CBZ Usage and Physicochemical Characteristics

CBZ is one of the most frequently used drugs for the medical treatment of epilepsy and bipolar disorder, being a mood stabilizer [4]. It is metabolized in the liver and excreted mainly as hydroxylated and conjugated metabolite and only around 5% as an unchanged drug [44]. The formula, structure, identifier (i.e., CAS number) and the main physicochemical characteristics of CBZ are summarized in Table 1.

Table 1. Main CBZ physicochemical characteristics.

CAS n.	Formula	Structure	Molecular Wight	pK$_a$	Log K$_{OW}$	K$_H$	S
298-46-4	C$_{15}$H$_{12}$N$_2$O		236.274 g/mol	2.3 [45] 13.9 [46]	2.45 [9]	2.24 × 10^{10} atm·m^3/mol [47] ^{P}	0.0005 mol/L [9] at 18 mg/L and 25 °C [46]

CAS n.: Chemical Abstracts Service number; Formula: Chemical formula; pK$_a$: log of acid dissociation constant; Log K_{ow}: log of octanol-water partition coefficient; K$_H$: Henry's law constant; S: water solubility; ^{P}: predicted value.

CBZ is not considered a volatile compound and it is characterized by a value of the octanol-water partitioning coefficient below 3 which entails that it is moderately hydrophobic; it is also considered soluble in water based on the available values of the solubility. Moreover, in the aquatic environment and most of the water and wastewater treatment processes, CBZ is present as a non-ionized form, since its pK$_a$ is far from neutral, which is the usual pH condition for these treatments [48]. All these characteristics proved that CBZ is refractory to the traditional water and wastewater treatment processes and particularly to biological processes, as reported by several authors [3,5–7]. As a consequence, it is usually found in the effluent of the treatment plants and then in the surface water bodies where it is frequently released. The NORMAN Network database, which includes 20 countries and 25,359 samples, shows that the frequency of detection in this environmental matrix is about 73% [9]. The frequent occurrence of CBZ in the aquatic environment represents a relevant and concerning matter since this substance has adverse toxicological effects [4]. Indeed, CBZ is classified as a toxic compound concerning marine and surface water compartments, being the lowest predicted no effect concentration (PNEC) below 0.1 μg/L in both compartments (0.005 μg/L and 0.05 μg/L, respectively) according to the criteria proposed by NORMAN Prioritization framework for emerging substances and the REACH regulation [9,49]. Thus, CBZ represents a risk for the environment, but also for human health when surface water is used as a source for drinking water production.

3. Presence and Fate in Water Treatment Plants (WTPs)

3.1. Wastewater Treatment Plants (WWTPs)

As seen in Section 2, CBZ is used as an antiepileptic drug, then excreted as such or as metabolites by the human body and it ends up in wastewaters. Frequency of detection (Fd) is the parameter of relevance when evaluating the pollution of water by a contaminant that describes the steadiness of its occurrence. For CBZ, its frequency of detection is often significantly high, defining pollution not randomly but consistently present in wastewater influent and effluent. On this account indeed, Loos et al. (2013) reported a frequency of detection of 90% in WWTPs effluent sampled across the EU [50]; Di Marcantonio et al. (2020) found an Fd of 96% and 91% in the influent and effluent, respectively [3]. According to Thiebault et al. (2017), Suebdi et al. (2015), Tran and Gin (2017) and Rivera-Jaimes et al. (2018), 100% Fd was recorded in both influent and effluent [7,51–53]. Table 2 lists the average concentrations at which CBZ was found across the world in the influent and effluent of wastewater treatment plants: even if the values are often in the range of ng/L, there are also exceptions with concentrations reaching the order of magnitude of μg/L.

Table 2. CBZ concentration (ng/L) mean and range in WWTPs worldwide, considering raw wastewater (RWW) and treated wastewater (TWW).

Location	n° WWTPs	RWW (Mean/*Median*)	RWW Range	TWW (Mean/*Median*)	TWW Range	Ref.
China	5×	45	24–72	34	24–49	[54]
China		17	n.a.	18	n.a.	[55]
China		14	10–20	16	13–21	[56]
USA	2× *	193	61–588	289	91–731	[52]
USA	5×	115	34–350	21	<LOQ-62	[57]
Canada	5×	757	n.a.	713	n.a.	[58]
Mexico	*	214	85–380	285	165–476	[53]
Singapore	*	323	323–339	313	262–336	[7]
Spain		<LOQ	n.a.	97	n.a.	[59]
Spain	(WWTP1) *	166	69–283	102	29–198	[60]
	(WWTP2) *	172		140		
Spain	4× *	422	70–970	100	60–150	[61]
Turkey	5× *	19	<LOQ-95	5	<LOQ-75	[62]
Italy		570	n.a.	370	n.a.	[63]
Italy	76×	209	<LOQ-1381	193	<LOQ-890	[3]
Italy		140	n.a.	179	n.a.	[64]
Switzerland		256	n.a.	251	n.a.	[64]
Czech Republic		460	210–710	510	220–730	[65]
France		215	51–937	163	5–357	[51]
Germany		1536	246–815	1614	1020–2309	[66]
Germany	6×	*1900*	1500–2100	2000	1800–2200	[67]
Portugal	2×	*470*	440–500	520	500–540	[67]
Portugal	2×	*95*	47–226	117	62.7–245	[68]
African countries	(review)		117–6145		64–1438	[69]
India		1642	22–8200	393	88–900	[70]

Data shown are either reported as such in the articles or calculated with the data available (*). The data reported in Italic are medians. When needed, WebPlotDigitizer was used to gain data from graphs.

Regarding time-related patterns for CBZ pollution of wastewaters, seasonality is usually excluded, being CBZ a substance not linked to seasonal illness; moreover, daily patterns have not been detected [71]. However, some studies report that drier seasons exerted an influence on the CBZ concentration detected at WWTPs due to lower dilution, particularly in the case of combined sewers [4].

The behavior of CBZ in WWTPs has been well addressed in the reviews by Couto et al. (2019) [71] and Krzeminski et al. (2019) [72], along with other contaminants of emerging concern (CECs). WWTPs are not (yet) designed to remove CECs, which are hence often discharged in the receiving water body through the treated effluent [71]. Particularly, CBZ seems quite refractory to biological treatments [59,72]; furthermore, it is also not expected to adsorb greatly on solids (medium-low octanol-water partition coefficient) [71] and therefore these can explain the poor removal in WWTPs [6]. The removal reported for CBZ is often even negative, due to recombination processes of precursors, accumulation within the plant, release by solids and sampling strategies that do not consider the plant Hydraulic Retention Time (HRT) [3,7,71,73]. Regarding the influence of the WWTP layout, an interesting study is the one conducted by Di Marcantonio et al. (2020) [3], where 76 WWTPs were analyzed for 2.5 years. According to the results, CBZ showed very low removal efficiencies (lower than 50%), the lowest being recorded for layouts comprising secondary treatments alone, slightly improving where primary or tertiary treatments were also included. Indeed, the review by Yang et al. (2017) and that of Hai et al. (2018) also confirmed the scarce removal by the secondary treatment, regardless of the system used (Conventional Activated Sludge, membrane bioreactor, others) [4,74].

3.2. Drinking Water Treatment Plants (DWTPs)

As a consequence of the entrance of CBZ in drinking water sources through the pathway already described in Section 3.1, pollution of water sources occurs at every

level [75], including groundwaters [76]. Indeed, CBZ is detected at the influent of DWTPs, as shown in Table 3, as in the effluents.

Table 3. CBZ concentration (ng/L) mean and maximum and Fd (%) in DWTPs worldwide.

Location	n° DWTPs	Water Source	RW			TW			Ref.
			Fd	Mean/*Median*	Max	Fd	Mean/*Median*	Max	
Canada	17×	GW/SW	50	*3*	749	25	*0.21*	601	[77]
Canada	5× *	SW	68	3.1	7.2	65.6	1.92	3.6	[78]
USA		SW	13	1.4	1.6	13	0.3	0.4	[79]
USA	31× *	GW/SW	37	6.1	17.9	27	3.6	6.9	[80]
USA	29×	GW/SW	56	*15.9*	35.7	8	*17.75*	26.5	[81]
Japan	6× *	GW/SW	39	7.3	100	13	1.9	25	[82]
Korea	5×	SW	100	7.7	21.1	5	0.67	0.67	[83]
Korea		SW	92	10.3	46.4	13	1.7	17.7	[84]
China		SW	100	1.33–1.82		100	0.37–1.15		[85]
China		SW	100	0.8	1.01	13	n.a.	0.65	[86]
Sweden	90×	GW/SW	41.5	0.95	n.a.	35	0.95	n.a.	[87]
Sweden	7× *	SW	100	10.48	13.44	28.5	2.91	11.32	[88]
Spain	*	SW	92	153	245	8.3	0.02	0.09	[89]
Spain	*	GW	100	*84.5*	167	89	1.1	5.7	[90]
Italy	3× *	SW	66.6	13.8	34.57	41.7	0.2	1.20	[91]
Portugal		GW/SW	96	3.3	16.8	69	1.8	13.5	[92]

Data shown are either reported as such in the articles or calculated with the data available (*). Fd: frequency of detection (%), GW: groundwater, n.a.: not available, RW: raw water, SW: surface water, TW: treated water. Values in italics are medians; when needed, WebPlotDigitizer was used to gain data from graphs.

The frequency of detection (%) is often quite high and not necessarily decreasing between influent and effluent of the water treatment plant, highlighting the persistence of the compound. The Fd median value, considering the studies reported in Table 3, for raw water is 80%, whereas for treated water it is 25%. The concentration in the effluent is usually lower, confirming at least a partial effect of the water treatment units. The concentrations reported by worldwide example studies in Table 3 show quite a variability: in raw water, the range spans from almost zero to hundreds of ng/L, whereas in treated water it is reduced to tens of ng/L. However, the presence of CBZ at the effluent of DWTPs is common to different countries and plant layouts. In general, treatments for the removal of colloids and solids are indeed not deemed to be effective against CBZ due to its characteristics, while improved outcomes might be linked to chemical oxidation processes such as ozonation, adsorptive process by granular activated carbon (GAC) and membrane filtration [71].

Simazaki et al. (2015) found that the average removal of CBZ by plants that included ozonation and activated carbon was of 97 ± 2%, whereas the removal was reduced to 62 ± 49% where such processes were not applied [82]. The importance of the oxidation steps in the removal of CBZ is also underlined by Kim et al. (2020) [83]. Pulicharla et al. (2021) found instead the removal of CBZ to be as low as 0–40% even in DWTPs with a layout that included inter-ozonation, activated carbon and sand filtration [78].

High removal efficiencies were also recorded for DWTPs employing Granular Activated Carbon (GAC) and Biological Activated Carbon (BAC) in Italy [91], even though concentration was not always reduced to below the limit of quantification (LOQ). The high removal of CBZ by nanofiltration/reverse osmosis (NF/RO) was instead witnessed by Radjenović et al. (2008) [90] and Al-rifai et al. (2011) [93].

4. Carbon-Based Sorbent

4.1. Activated Carbon

Activated carbon (AC) is an amorphous carbon-containing material with a highly porous structure [94] and a large specific surface area [95]. Thanks to these properties, AC presents a great ability to remove molecules or other substances, from water and

wastewater [96–100]; the first applications were developed in the field of drinking water, as for smell removal [101]. Generally, AC can be found in two forms:

- granular activated carbon (GAC): it is made up of particles of a size comparable to that of sand (between 0.2 and 5.0 mm) and is used when a material with larger pores and a smaller specific surface is required [102,103];
- powdered activated carbon (PAC): it is formed by the most minute particles (smaller than 0.2 mm) and is used when small particles are needed with greater specific surface area [104,105].

AC production starts with the carbonization of raw materials with high carbon content, in order to produce the chars, followed by a physical or chemical, or physico-chemical activation process [106,107].

Physical activation is conducted at high temperatures (between 800 °C and 1000 °C), in the presence of an oxidizing agent such as O_2, CO_2, steam or a gaseous mixture [108].

Chemical activation is based on the dehydrating action of some chemicals, such as $CaCl_2$, HCl, H_2SO_4, H_3PO_4, HF, KOH, NaOH and $ZnCl_2$ [109,110].

4.2. Biochar

Biochar (BC) is a solid product obtained from different types of vegetable biomass or organic waste through a thermal convection process, in the absence or limited presence of oxygen [111,112]. The origins of BC can be traced back to the Amazon, where numerous sites known as "Terra Preta dos Indios" have been identified, where biochar was buried to increase their crops [113–115].

BC can be synthesized from one of the well-known carbonization processes [116] such as pyrolysis [117], pyro-gasification [118], gasification [119], hydrothermal carbonization [111], torrefaction [120], microwave pyrolysis [121], mechanochemical technology [122], functionalization/activation or engineering [123], etc.

BC, thanks to its high carbon content and porosity, is a powerful soil improver [124]. It can therefore be used in the agriculture sector [125]: several studies show the positive impact of BC on agricultural yield [126], with an improvement in the biological fertility of the soil [127] which implies less consumption of water and chemical fertilizers [128]. This involves a lower environmental impact [129] and lower consumption of natural resources and energy [130]. It can also be used in the horticultural sector [131]: its main action is to make the nutrients needed for plants' growth [132], specifically, calcium, magnesium, potassium and nitrogen, always available [133,134]. Moreover, BC helps to maintain the optimal pH of soil for plants activities [135].

The production of BC is also a sustainable solution for waste management [136,137] since it sequesters CO_2 [138], reintroduces important elements into the environment [139,140], replaces highly polluting materials and allows contributing to the circular economy [141–143]. Recently, the application of BC as an adsorbent media has been suggested for the removal of several contaminants [144,145], both inorganic (metals, salts) and organic (insecticides, herbicides, antibiotics) [146–148], also including the emerging ones [149].

4.3. Characterization of Carbon-Based Adsorbents

The textural characteristic and elemental composition of activated carbon and biochar depend on the feedstock, temperature of pyrolysis and activation method. Looking at Table 4 it is possible to note the mains difference regarding their characteristic S_{BET} and C% which are higher in activated carbon than in biochar, while Ash content and N% are lower.

Table 4. Range of main physico-chemical parameters of activated carbon (AC) and biochar (BC).

Parameters	AC	References	BC	References
S_{BET} (m^2/g)	211–1910	[150–152]	0.9–470.4	[153]
V_{mi} (cm^3/g)	0.086–0.582	[151]	0.16–0.335	[154]
V_{me} (cm^3/g)	0.13–0.30	[155]	0.004–0.21	[154]
V_T (cm^3/g)	0.66–0.931	[150,156]	0.01–0.88	[154]
$\Lambda_{particle}$ (g/mL)	0.86–087	[45]	0.14–0.65	[157]
λ_{ap} (g/mL)	0.25–1.0	[158,159]	1.25–1.95	[157]
d (Å)	16–32	[160,161]	14–28	[162]
D (nm)	2.5–34	[163]	250–853	[164]
$IN°$ (mg/g)	402–822	[165]	446–1576	[162]
pH (-)	3.32–8.54	[166]	5.5–10.0	[157]
pH$_{PZC}$ (-)	4.02–9.92	[167]	7.0–9.5	[112,168]
Ash (%)	2.92–8.90	[154]	1.2–31.2	[157]
C (%)	82.81–83.46	[161]	1.7–90.9 51.8–81.9	[153,157]
N (%)	0.30–0.74	[161]	0.1–5.7	[157]
H (%)	0.32–2.05	[161]	0.3–4.3	[157]
O (%)	0.13–8.40	[166,169]	7.5–33.1	[157]

The following section described the theory of the textural properties and the elemental analyses.

4.3.1. BET Analysis

The main method for measuring the specific surface area and the distribution of the pores of a carbonaceous material is through the Brunauer, Emmett and Teller (BET) analysis, using precisely the BET theory that was initially developed to describe multilayer adsorption-desorption of gas molecules on a solid surface of the adsorbent material [170,171].

The BET analysis is performed based on the adsorption isotherms of non-reactive gas molecules (such as N$_2$, CO$_2$ or Ar at 77 °K, 273 °K and 87 °K, respectively) in a range of pressure values that refer to the monolayer coverage of molecules.

Samples are commonly prepared by heating them in a vacuum or under a gas stream to remove impurities. The samples are then analyzed by measuring the volume of adsorbed gas.

Models and mathematical simulations are applied to the results of the BET analysis, which allow information to be obtained regarding the specific surface area and the distribution of pores in the material.

Specific Surface Area

Specific surface area (SSA) of carbon-based sorbents is a fundamental property that has a decisive impact on the adsorption mechanism of contaminants [171]. To determine the SSA (S_{BET}, m^2/g), the BET theory is applied, through the nonlinear form of Equation (1) [172]:

$$\frac{V}{V_m} = \frac{C\left(\frac{P}{P_0}\right)}{\left[1 + (C-1)\left(\frac{P}{P_0}\right)\right]\left[1 - \left(\frac{P}{P_0}\right)\right]} \tag{1}$$

where P/P_0 is the relative pressure of adsorbate (-), V (cm^3), V_m (cm^3) and C (-) are the volume filled by multilayer adsorption on the external surface, the volume of a monolayer

and the BET isotherm constant, respectively [173]. The linearized form of Equation (1) is described below [174]:

$$\frac{\left(\frac{P}{P_0}\right)}{\left[V\left(1 - \frac{P}{P_0}\right)\right]} = \frac{1}{CV_m} + \frac{(C-1)\left(\frac{P}{P_0}\right)}{CV_m} \tag{2}$$

Both parameters C and V_m can be estimated from the slope and intercept of the linear form of the equation. The plots of linearized variables provide straight lines at low relative pressure (P/P_0) range, as shown in Table 5, depending on the sample.

Table 5. Range of P/P_0 at the low-pressure range.

Range of P/P_0	Ref.
0.05–0.30	[171,175]
0.05–0.25	[174]
0.10–0.26	[176]

The C constant is described by Equation (3):

$$C = \left(\frac{\alpha_1 \nu_2}{\alpha_2 \nu_1}\right) exp\left[\frac{(q_1 - q_L)}{RT}\right] \tag{3}$$

where α_i and ν_j are the condensation coefficient and the frequency of oscillation of the molecules, respectively, for the first (i, j = 1) and the second layers (i, j = 2), q_1 and q_L are the heat of adsorption in the first layer (on the bare surface) and the heat of condensation of all other layers, respectively, which is the same among all, except for the first [174].

Kembal and Schreiner [177] suggested that the coefficient of the exponential $(\alpha_1\nu_2/\alpha_2\nu_1)$ can be considered approximately as the unit value. Thus, the BET constant corresponds approximately to the value of the C-parameter at the point where the adsorbed monolayer is formed.

The analysis of the experimental BET adsorption isotherms and these simplifications allow determining sorption capacities (V_m) using the following Equation (4) [178]:

$$V_m = V\left(1 - \frac{P}{P_0}\right) \tag{4}$$

Finally, the SSA $(S_{BET}, m^2/g)$ can be quantified using Equation (5) [175,178]:

$$S_{BET} = \frac{V_m \sigma_0 N_{AV}}{m} \frac{\rho_{GAS}}{M_{GAS}} = V_m \frac{s_m}{m} \tag{5}$$

where σ_o and N_{AV} are the cross-sectional area of non-reactive gas (m^2) and the Avogadro number (6.022×10^{23} L/mol), respectively; ρ_{GAS} and M_{GAS} are the density and the molecular mass of gas, respectively; m is the weight of the sample of the carbon-based sorbents (g).

Micropore and Mesopore Volumes

Available methods for measuring micropore distribution include Density Functional Theory (DFT), MP-Method, Dubinin Plots (Dubinin–Radushkevich D-R, Dubinin–Astakov D-A) and Horvath–Kawazoe (H-K). As for instead, mesopore methods available include the Barrett, Joyner and Halenda method (BJH) and Density Functional Theory (DFT).

The methods developed by Dubinin and Radushkevich (1947) are the most common approaches to evaluate micropore volumes $(V_{mi}, cm^3/g)$ of carbon-based sorbent, assuming

them to obey a Gaussian distribution [179]. The DR nonlinear equation is described below [180]:

$$\frac{V_1}{V_{DR}} = \exp\left[-\left(\frac{E}{E_0}\right)^2\right] = \exp\left\{-\left(\frac{R_{GAS}T}{E_{DR}\beta}\right)^2\left[\ln\left(\frac{P_0}{P}\right)\right]^2\right\} \tag{6}$$

where V_1 is the micropore volume filled by gas (N_2, Ar or CO_2), R_{GAS} and T are the gas constant and analysis temperature (°K), respectively, β is the affinity coefficient, different for each gas, E_0 the characteristic energy (kJ) and E the adsorption energy (kJ), given by the Polanyi equation [RT $\ln(p/p_0)$].

Moreover, E_{DR} and V_{DR} represent the interaction energy and the limiting adsorbed volume, respectively; the following Equation (7) represents the DR linear form:

$$\ln(V_1) = \ln(V_{DR}) - \left(\frac{R_{GAS}T}{E_{DR}\beta}\right)^2\left[\ln\left(\frac{P_0}{P}\right)\right]^2 \tag{7}$$

Both parameters E_{DR} and V_{DR} can be determined from the slope and intercept of the straight line in the DR-plot ($\ln(V_1)$ vs. $(\ln(P_0/P))^2$), at very small relative pressures in the linear region (Table 5). Micropore volumes can be calculated as the intercept [181]:

$$V_{mi} = \exp[\ln(V_{DR})] \tag{8}$$

The mesopore volume (V_{me}, cm^3/g) can be calculated by subtracting the micropore volumes V_{mi} to the total pore volumes (V_T) [182,183]:

$$V_{me} = V_T - V_{mi} \tag{9}$$

4.3.2. Total Pore Volume

Total pore volume (V_T, cm^3/g) frequently can be derived from a nitrogen adsorption isotherm, through the BET analysis described in Section 4.1, under a certain relative pressure value (i.e., $P/P_0 \leq 0.998$) [150]. Experimentally, the study of adsorption isotherms uses the following Equation (10) [184]:

$$V_T = q_{sat}\frac{\rho_{vap}}{\rho_{liq}} \tag{10}$$

where q_{sat} is the loading at saturation expressed at standard pressure and temperature (mL/g); ρ_{vap} and ρ_{liq} are the density for the vapour phase at standard pressure and temperature and the liquid phase at normal boiling point, respectively. Analytically, the total pore volume can also be determined through Equation (11) [176]:

$$V_T = \frac{1}{\Lambda} - \frac{1}{\Lambda_{part}} \tag{11}$$

where Λ is the macroscopic density of the dried material (g/mL) sample and $\Lambda_{particle}$ is the effective particle density defined by Equation (12):

$$\Lambda_{particle} = \frac{1}{\frac{1}{\lambda_{ap}+V_{mi}}} \tag{12}$$

where λ_{ap} is the apparent density (g/mL), described below in Section 4.3.6, and V_{mi} is the specific micropores volume (cm^3/g), as previously described in Section 4.1.

The single, complete pore size distribution (CPSD) and total pore volume (V_T) also may be calculated from a model that combines model adsorption isotherms and mercury intrusion curves [185] or using the Barrett–Joiner–Halenda (BJH) equation [186,187].

4.3.3. Average Pore Width

Most of the porous materials are classified into four major groups based on their pore size [171]:

- ultra-micropores (<0.7 nm);
- micropores (<2 nm);
- mesopores (between 2 nm and 50 nm);
- macropores (>50 nm).

The average pore width (d, Å), can be analyzed by the Barrett–Joiner–Halenda (BJH) method [188] or calculated from specific external surface (S_{ext} = specific total area-specific area of micropores) and total specific pore volume (V_T), via Equation (13) that assumes cylindrical pores [176,189]:

$$d = \frac{4(V_T)}{S_{ext}} \tag{13}$$

4.3.4. Average Particle Size

The average size of the particles forming the carbon-based sorbents (μm) may be calculated from S_{ext} and the particle density ($\Lambda_{particle}$), assuming a spherical geometry [190], according to Equation (14):

$$D = 2\frac{3}{S_{ext}\Lambda_{part}} \tag{14}$$

4.3.5. Particle Density

The real density, or particle density ($\lambda_{particle}$, g/mL), is defined as the ratio between the mass and the volume of a sample, without considering pores in the material (true volume); in the case of granular or carbonaceous materials, the following Equation (15) is used, which also considers the particle density and particle volume [191]:

$$\lambda_{particle} = \frac{m_s + m_w}{v_s + v_w} \tag{15}$$

where m_s and m_w are the dry mass of sample and water mass, respectively; v_s and v_w are the solid and water volume of sample, respectively. The real density can be experimentally measured using appropriate methodologies, using instruments in which a helium volume cell is inserted (i.e., a pycnometer) [109,191,192]. Before being subjected to the analysis of the real density, the sample is dried at 105 °C, to eliminate the contribution related to water; the air volume will thus be increased by the evaporation of the water.

Measurement of the sample volume (v_{sample}) is performed by filling the sample cell with helium to the required filling pressure; then the gas expands in the cell (p_1) and the final pressure at equilibrium (p_2) are recorded. The sample volume is calculated according to Equation (16):

$$v_{sample} = v_{cell} - \frac{v_{exp\ cell}}{\left(\frac{p_1}{p_2}\right) - 1} \tag{16}$$

where v_{sample}, v_{cell} and $v_{exp\ cell}$ are the volume of the sample, the sample cell and the expansion cell (mL), respectively; p_1 and p_2 are the run fill pressure and the final pressure, respectively [192].

4.3.6. Apparent Density

Apparent density (or bulk density) (λ_{ap}, g/mL) can be deduced from the dimensions and weight of the carbonaceous material and by weighing a known volume of gently tapped AC or BC, including pores and water [109,193]:

$$\lambda_{ap} = \frac{m_s + m_w}{v_s + v_w + v_a} \tag{17}$$

where v_a is the air volume of the sample [192]. Moreover, wet ($\lambda_{ap,w}$) and dry ($\lambda_{ap,d}$) bulk density (g/mL) of all carbon-based sorbents can be determined using the same mass per unit volume technique; below are presented the Equations (18) and (19) for the determination of both densities [194]:

$$\lambda_{ap,w} = \frac{m}{v} \tag{18}$$

$$\lambda_{ap,d} = \rho_{bw}\frac{100 - wc}{100} \tag{19}$$

where m, v and wc are the weight (g), volume (mL) and moisture content (%) of the carbonaceous material, respectively.

4.3.7. Iodine Number

Iodine number ($IN°$) is one of the fundamental parameters used to characterize the adsorption on carbonaceous materials [195]. $IN°$ (mg/g) is the amount of iodine (in milligrams) adsorbed by 1.0 g of the carbon-based sorbent under standard conditions [175].

Several standard tests can be used for the determination of $IN°$, where, likewise, the amount of iodine remaining in the residual aqueous phase of the adsorption tests is measured [195,196]. Therefore, $IN°$ can be calculated using the following Equation (20):

$$IN° = \frac{v_B - v_T}{v_B}\frac{v_I}{mM_I} \tag{20}$$

where v_b, v_t and v_I are the volume of blank titration, the volume of test titration and volume of iodine solution used, respectively; M_I is the molarity of iodine solution and m is the weight of the carbon-based sorbents [197].

4.3.8. pH

To determine the pH value, a known quantity of carbonaceous material (i.e., 1.0 g) is mixed with a certain volume (mL) of distilled or ultrapure water (i.e., 100 mL) and subsequently, the pH is determined with a pH meter/specific probe [198].

4.3.9. Point of Zero Charge and Isoelectric Point

The point of zero charge (pH_{PZC}) is the pH value at which the net electric charge density on a material surface is zero. It is linked to the concept of isoelectric point (pH_{IEP}), from which it differs when the adsorption of ions by the surface is not zero [199].

Defined amounts of carbon-sorbent materials are put into contact with acidic or basic solutions with different molarities (i.e., 0.03 M KNO_3 [200] or 0.01 M NaCl [201]) and/or normality (i.e., 0.1 N HCl and 0.1 N NaOH [202]). The aqueous solution is stirred for 24 h in a shaker at 250 rpm, until equilibrium pH is reached.

Graphically, the point of zero charge (pH_{PZC}) is the point at which a plateau is achieved when plotting equilibrium pH versus sorbent mass (g or g/L).

4.3.10. Ash Content

For the determination of ash content (%), a known quantity of carbon-based sorbents (i.e., 1.0 g [203]) is weighed and dried using a muffle oven at about 500 °C and subsequently cooled in the dryer. Then, the % ash content (dry basis) is calculated from Equation (21) [198]:

$$Ash(\%) = \frac{m_{°C}}{m_s}100 \tag{21}$$

where $m_{°C}$ and m_s are the weight of the sample after and before ash process, respectively.

4.3.11. Elemental Composition

The elemental composition of carbon-based sorbents is highly dependent on feedstock and conditions of the production process [187].

Analysis of the elemental composition of the carbonaceous material through, i.e., elemental analyzer [187,204,205] or X-ray fluorescence spectroscopy (XRF) [206,207], is performed to establish the weight fractions of elements (i.e., C, N, H, S, O, Na and P) in the sample.

Furthermore, molar ratios (i.e., H/C, O/C, C/N and (O + N)/C) can be subsequently also calculated. These ratios provide an indication of the properties and the thermal convection process production efficiency of the material [187].

4.3.12. Adsorption Capacity

The amount of a pollutant adsorbed onto a carbon-based sorbent, which represents the adsorption capacity, q (mg/g), can be determined experimentally by Equation (22):

$$q = \frac{(C_0 - C)}{m} V \ or \ \frac{(C_0 - C)}{D_{l/s}} \tag{22}$$

where C_0, C and C_e (mg/L) are concentration at t = 0, at time t and at equilibrium, respectively; V and m are the volume of solution (L) and the mass of adsorbent (g), respectively, or the liquid–solid ratio ($D_{l/s}$) of carbon-based sorbent (g/L) [208].

5. Adsorption of CBZ onto Carbon-Based Adsorbents

Table 6 summarizes the main experimental conditions and results of some of these studies. In the next sections, these data will be discussed, as well as the relation between physicochemical properties, operational parameters and CBZ adsorption, kinetics and isotherms and removal mechanisms.

This section reports on the effects of the adsorbent properties and operational conditions on CBZ adsorption. Afterwards, the main kinetic and isotherm models applied to this process are presented and discussed.

Table 6. CBZ adsorption in water solution by activated carbon and biochar: batch studies.

Adsorbent Medium	Feedstock	Modification/ Activation	Physico-Chemical Properties	Kinetic Studies				Isotherm Studies			Mechanism	Ref.
				Operational Condition	t_e (h)	q_e (mg/g)/R (%)	Kinetics Model	Operational Condition	Parameter	Isotherms Model		
GAC Calgon Filtrasorb 400 (F400)	Bituminous coal	n.a.	$\Lambda_{particle}$: 0.85 g/mL λ_{ap}: 0.44 g/mL $IN°$: 1000 mg/g S_{BET}: 1030 m²/g	n.a.	n.a.	n.a.	n.a.	SR: 120 rpm T: 23 ± 1 °C C_0: 1 µg/L Dosage: 1–10 mg/L t: 288 h	K_F: 73.79 (ng/mg) (L/ng)$^{1/n}$	Freundlich	n.a.	[45]
GAC PICACTIF TE (PICA)	Coconut shell	n.a.	$\Lambda_{particle}$: 0.86 g/mL λ_{ap}: 0.51 g/mL $IN°$: 1237 mg/g S_{BET}: 1156 m²/g	n.a.	n.a.	n.a.	n.a.	SR: 120 rpm T: 23 ± 1 °C C_0: 1 µg/L Dosage: 1–10 mg/L t: 288 h	K_F: 57.56 (ng/mg) (L/ng)$^{1/n}$	Freundlich	n.a.	[45]
GAC Calgon Filtrasorb 400 (F400)	Bituminous coal	n.a.	$IN°$: 1000 mg/g	SR: 120 rpm T: 24 ± 1 °C pH: 7 C_0: 1 µg/L Dosage: 5 mg/L	144	n.a.	n.a.	SR: 120 rpm T: 24 ± 1 °C pH: 7 C_0: 1 µg/L Various dosage t: 288 h	q_m: 2.719 mg/g	Sips	n.a.	[209]
GAC PICACTIF TE (PICA)	Coconut shell	n.a.	$IN°$: 1237 mg/g	SR: 120 rpm T: 24 ± 1 °C pH: 7 C_0: 1 µg/L Dosage: 5 mg/L	n.a.		n.a.	SR: 120 rpm T: 24 ± 1 °C pH: 7 C_0: 1 µg/L Various dosage t: 288 h	q_m: 571.7 mg/g	Sips	n.a.	[209]
Activated carbon PC	Peach stone	Activation: H_3PO_4	S_{BET}: 1216 m²/g V_T: 0.81 cm³/g V_{mi}: 0.56 cm³/g V_{me}: 0.25 cm³/g pH$_{IEP}$: 3.2 ± 0.25 pH$_{PZC}$: 3.1	SR: 250 rpm T: 30 °C C_0: 100 mg/L Dosage: 2400 mg/L	2–3	$q_{e\ exp}$: 30	n.a.	SR: 250 rpm T: 30 °C C_0: 100 mg/L Various dosage	q_m: 14,234 mg/g	Sips	n.a.	[182]

Table 6. *Cont.*

Adsorbent Medium	Feedstock	Modification/ Activation	Physico-Chemical Properties	Kinetic Studies				Isotherm Studies			Mechanism	Ref.
				Operational Condition	t_e (h)	q_e (mg/g)/R (%)	Kinetics Model	Operational Condition	Parameter	Isotherms Model		
Activated carbon O-PC	Peach stone	Activation: H_3PO_4 Modification: HNO_3	S_{BET}: 959 m^2/g V_T: 0.57 cm^3/g V_{mi}: 0.42 cm^3/g V_{me}: 0.14 cm^3/g pH$_{IEP}$: 2.5 ± 0.25 pH$_{PZC}$: 2.1	SR: 250 rpm T: 30 °C C_0: 100 mg/L Dosage: 2400 mg/L	2–3	n.a.	n.a.	SR: 250 rpm T: 30 °C C_0: 100 mg/L Different dosage	q_m: 2456 mg/g	Sips	n.a.	[182]
Activated carbon He-PC	Peach stone	Activation: H_3PO_4 Modification: He flow	S_{BET}: 1064 m^2/g V_T: 0.65 cm^3/g V_{mi}: 0.46 cm^3/g V_{me}: 0.18 cm^3/g pH$_{IEP}$: 3.4 ± 0.25 pH$_{PZC}$: 4.3	SR: 250 rpm T: 30 °C C_0: 100 mg/L Dosage: 2400 mg/L	2–3	n.a.	n.a.	SR: 250 rpm T: 30 °C C_0: 100 mg/L Various dosage	q_m: 224 mg/g	Sips	n.a.	[182]
PAC	n.a.	n.a.	S_{BET}: 470.1 m^2/g	SR: 100 rpm C_0: 23630 µg/L * Dosage: 100 mg/L	2	$q_{e\ calc}$: 71.9	PS0	n.a.	n.a.	n.a.	n.a.	[210]
Activated carbon AC-RH	Rice husk	chemical activation with H_3PO_4	S_{BET}: 278 m^2/g V_T: 0.26 cm^3/g V_{mi}: 0.14 cm^3/g V_{mi}/V_T: 0.538 pH$_{PZC}$: 3.3	SR: 250 rpm T: 30 °C pH: 6.5 C_0: 100 mg/L Dosage: 2400 mg/L	4	$q_{e\ exp}$: 170.3		SR: 250 rpm T: 30 °C pH: 6.5 C_0: 100 mg/L Dosage: 200–20,000 mg/L	q_m: 45,000 mg/g q_m: 26 mg/g	Sips GAB	pore-filling	[211]
Activated carbon AC-PS	Peach stones	chemical activation with H_3PO_4	S_{BET}: 1521 m^2/g V_T: 0.90 cm^3/g V_{mi}: 0.52 cm^3/g V_{mi}/V_T: 0.578 pH$_{PZC}$: 3.1	SR: 250 rpm T: 30 °C pH: 6.5 C_0: 100 mg/L Dosage: 2400 mg/L	4	$q_{e\ exp}$: 241.7		SR: 250 rpm T: 30 °C pH: 6.5 C_0: 100 mg/L Dosage: 200–20,000 mg/L	q_m: 4344.7 mg/g q_m: 310.2 mg/g	Sips (Langmuir–Freundlich) GAB	pore-filling	[211]

Table 6. *Cont.*

Adsorbent Medium	Feedstock	Modification/ Activation	Physico-Chemical Properties	Kinetic Studies				Isotherm Studies			Mechanism	Ref.
				Operational Condition	t_e (h)	q_e (mg/g)/R (%)	Kinetics Model	Operational Condition	Parameter	Isotherms Model		
GAC Calgon Filtrasorb 400 (F400)	Bituminous coal		S_{BET}: 1102 m^2/g V_T: 0.58 cm^3/g V_{mi}: 0.46 cm^3/g V_{mi}/V_T: 0.793 pH$_{PZC}$: 7.6–7.9	SR: 250 rpm T: 30 °C pH: 6.5 C_0: 100 mg/L Dosage: 2400 mg/L	4	$q_{e\ exp}$: 220.2		SR: 250 rpm T: 30 °C pH: 6.5 C_0: 100 mg/L Dosage: 200–20,000 mg/L	q_m: 1554.3 mg/g q_m: 131.3 mg/g	Sips GAB	pore-filling	[211]
BC200 Biochar	Peanut shells	n.a.	S_{BET}: 1.827 m^2/g V_T: 0.010 m^3/g Ash: 10.827% C: 46.105% N: 0.988% H: 5.264% S: 0.404% O: 36.414% H/C: 1.370 (O + N)/C: 0.61	SR: 12 rpm T: RM pH: 6.4–6.6 C_0: 13 mg/L Dosage: 5; 2.5 and 1.25 mg/L *	168	$q_{e\ calc}$: 1034.20	2-CFOSM	SR: 12 rpm T: RM C_0: 1.0–50 mg/L Dosage: 1.25, 2.5 and 5 mg/L *	q_m: 5.51 mg/g *	Dubinin–Astakhov	Hydrophobic interaction π-π bonding interactions	[212]
HBC200 Biochar	Peanut shells	HCl 1 M washed	S_{BET}: 1.619 m^2/g V_T: 0.010 m^3/g Ash: 8.784% C: 47.120% N: 0.679% H: 5.469% S: 0.000% O: 37.948% H/C: 1.393 (O + N)/C: 0.616	SR: 12 rpm T: RM pH: 6.4–6.6 C_0: 13 mg/L Dosage: 5; 2.5 and 1.25 mg/L *	168	$q_{e\ calc}$: 1067.60	2-CFOSM	SR: 12 rpm T: RM t: 168 h C_0: 1.0–50 mg/L Dosage: 1.25, 2.5 and 5 mg/L *	q_m: 12.76 mg/g *	Dubinin–Astakhov	Hydrophobic interaction π-π bonding interactions	[212]
FBC200 Biochar	Peanut shells	HCl/HF 1:1 1 M washed	S_{BET}: 1.435 m^2/g V_T: 0.010 m^3/g Ash: 6.530% C: 49.395% N: 0.763% H: 5.688% S: 0.031% O: 37.593% H/C: 1.382 (O + N)/C: 0.584	SR: 12 rpm T: RM pH: 6.4–6.6 C_0: 13 mg/L Dosage: 5; 2.5 and 1.25 mg/L *	168	$q_{e\ calc}$: 841.82	2-CFOSM	SR: 12 rpm T: RM t: 168 h C_0: 1.0–50 mg/L Dosage: 1.25, 2.5 and 5 mg/L *	q_m: 4.88 mg/g *	Dubinin–Astakhov	Hydrophobic interaction π-π bonding interactions	[212]

Table 6. *Cont.*

Adsorbent Medium	Feedstock	Modification/ Activation	Physico-Chemical Properties	Kinetic Studies				Isotherm Studies			Mechanism	Ref.
				Operational Condition	t_e (h)	q_e (mg/g)/R (%)	Kinetics Model	Operational Condition	Parameter	Isotherms Model		
BC300 Biochar	Peanut shells	n.a.	S_{BET}: 7.088 m^2/g V_T: 0.018 m^3/g Ash: 14.852% C: 54.945% N: 1.572% H: 3.517% S: 0.259% O: 24.844% H/C: 0.768 (O + N)/C: 0.364	SR: 12 rpm T: RM * pH: 6.4–6.6 C_0: 13 mg/L Dosage: 5; 2.5 and 1.25 mg/L *	168	$q_{e\ calc}$: 2259.48	2-CFOSM	SR: 12 rpm T: RM t: 168 h C_0: 1.0–50 mg/L Dosage: 1.25, 2.5 and 5 mg/L *	q_m: 6.39 mg/g *	Dubinin– Astakhov	Hydrophobic interaction π-π bonding interactions	[212]
HBC300 Biochar	Peanut shells	HCl 1 M washed	S_{BET}: 3.098 m^2/g V_T: 0.012 m^3/g Ash: 10.415% C: 56.913% N: 1.428% H: 3.864% S: 0.047% O: 27.333% H/C: 0.815 (O + N)/C: 0.382	SR: 12 rpm T: RM * pH: 6.4–6.6 C_0: 13 mg/L Dosage: 1.25, 2.5 and 5 mg/L *	168	$q_{e\ calc}$: 1402.54	2-CFOSM	SR: 12 rpm T: RM t_e: 168 h C_0: 1.0–50 mg/L Dosage: 1.25, 2.5 and 5 mg/L *	q_m: 14.81 mg/g *	Dubinin– Astakhov	Hydrophobic interaction π-π bonding interactions	[212]
FBC300 Biochar	Peanut shells	HCl/HF 1:1 1 M washed	S_{BET}: 2.693 m^2/g V_T: 0.011 m^3/g Ash: 7.970% C: 58.321% N: 1.128% H: 4.113% S: 0.046% O: 28.421% H/C: 0.846 (O + N)/C: 0.381	SR: 12 rpm T: RM * pH: 6.4–6.6 C_0: 13 mg/L Dosage: 1.25, 2.5 and 5 mg/L *	168	$q_{e\ calc}$: 1121.81	2-CFOSM	SR: 12 rpm T: RM t: 168 h C_0: 1.0–50 mg/L Dosage: 1.25, 2.5 and 5 mg/L *	q_m: 6.84 mg/g *	Dubinin– Astakhov	Hydrophobic interaction π-π bonding interactions	[212]

Table 6. *Cont.*

Adsorbent Medium	Feedstock	Modification/ Activation	Physico-Chemical Properties	Kinetic Studies				Isotherm Studies			Mechanism	Ref.
				Operational Condition	t_e (h)	q_e (mg/g)/R (%)	Kinetics Model	Operational Condition	Parameter	Isotherms Model		
BC500 Biochar	Peanut shells	n.a.	S_{BET}: 64.728 m^2/g V_T: 0.057 m^3/g Ash: 16.857% C: 59.448% N: 1.603% H: 2.710% S: 0.264% O: 19.117% H/C: 0.547 (O + N)/C: 0.264	SR: 12 rpm T: RM * pH: 6.4–6.6 C_0: 13 mg/L Dosage: 1.25, 2.5 and 5 mg/L *	168	$q_{e\ calc}$: 2997.62	2-CFOSM	SR: 12 rpm T: RM t: 168 h C_0: 1.0–50 mg/L Dosage: 1.25, 2.5 and 5 mg/L *	q_m: 5.38 mg/g *	Dubinin– Astakhov	Hydrophobic interaction π-π bonding interactions	[212]
HBC500 Biochar	Peanut shells	HCl 1 M washed	S_{BET}: 72.251 m^2/g V_T: 0.061 m^3/g Ash: 11.489% C: 66.339% N: 1.467% H: 28.14% S: 0.020% O: 17.870% H/C: 0.509 (O + N)/C: 0.221	SR: 12 rpm T: RM * pH: 6.4–6.6 C_0: 13 mg/L Dosage: 1.25, 2.5 and 5 mg/L *	168	$q_{e\ calc}$: 2681.05	2-CFOSM	SR: 12 rpm T: RM t: 168 h C_0: 1.0–50 mg/L Dosage: 1.25, 2.5 and 5 mg/L *	q_m: 4.96 mg/g *	Dubinin– Astakhov	Hydrophobic interaction π-π bonding interactions	[212]
FBC500 Biochar	Peanut shells	HCl/HF 1:1 1 M washed	S_{BET}: 85.072 m^2/g V_T: 0.069 m^3/g Ash: 8.260% C: 69.090% N: 1.407% H: 3.002% S: 0.052% O: 18.189% H/C: 0.521 (O + N)/C: 0.215	SR: 12 rpm T: RM * pH: 6.4–6.6 C_0: 13 mg/L Dosage: 5; 2.5 and 1.25 mg/L *	168	$q_{e\ calc}$: 2510.47	2-CFOSM	SR: 12 rpm T: RM t: 168 h C_0: 1.0–50 mg/L Dosage: 1.25, 2.5 and 5 mg/L *	q_m: 3.95 mg/g *	Dubinin– Astakhov	Hydrophobic interaction π-π bonding interactions	[212]

Table 6. *Cont.*

Adsorbent Medium	Feedstock	Modification/ Activation	Physico-Chemical Properties	Kinetic Studies				Isotherm Studies			Mechanism	Ref.
				Operational Condition	t_e (h)	q_e (mg/g)/R (%)	Kinetics Model	Operational Condition	Parameter	Isotherms Model		
Activated carbon PKS	Palm kernel shell	CO_2 activation	S_{BET}: 711.5 m^2/g V_T: 0.419 cm^3/g V_{mi}: 0.2355 cm^3/g V_{me}: 0.1835 cm^3/g pH$_{pzc}$: 11.5	SR: 250 rpm T: 25 °C pH: 7 C_0 (mg/L): 100 150 200 250 Dosage: 1000 mg/L	4	$q_{e\ exp}$ (*) 136.88 122.72 110.92 84.96 92.04	Ritchie 2nd order Diffusion-chemisorption model	SR: 250 rpm T: 25 °C pH: 7 C_0: Different initial concentration Dosage: 1000 mg/L t: 24 h	q_m: 162.84 mg/g *	Sips	Hydrophobic interaction π-π bonding interactions	[201]
Mesoporous Activated carbon (Meso-AC 1)	n.a.	n.a.	S_{BET}: 214 m^2/g V_{me}: 0.43 cm^3/g V_{mi}: 0.008 cm^3/g	T: 25 ± 2 °C pH: 5.8–6 C_0: 50 mg/L Dosage: 100 mg/L	30	q_e: 180	n.a.	T: 25 ± 2 °C pH: 5.8–6 C_0: 50 mg/L Dosage: 100 mg/L	q_m: 191.55 mg/g	Brouers–Sotolongo	Hydrophobic interaction π-π bonding interactions	[186]
PAC Biopack	Vegetable origin	n.a.	S_{BET}: 1328.3 m^2/g λ_{ap}: 0.25 g/mL d: 13 Å V_T: 1.06 cm^3/g	SR: 90 rpm T: 25 °C pH: 6.15 C_0 (mg/L): 15 20 25 30 35 40 Dosage: 100 mg/L	72	$q_{e\ calc}$: 161 ± 4 204 ± 10 247 ± 13 260 ± 13 273 ± 11 297 ± 18	PSO	SR: 90 rpm T: 25 °C pH: 6.15 C_0: 10–40 mg/L Dosage: 100 mg/L t: 72 h	q_m: 220 ± 51 mg/g	Redlich–Peterson	n.a.	[159]
Nano Biochar (BC-PW)	Pine white wood	n.a.	S_{BET}: 47.25 m^2/g Ash: 2 ± 0.1% D: 0.06 μm C: 83.1 ± 2.5% H: 3.5 ± 0.11% N: <1% H/C: 0.5 C/N: >96.5 pH: 6.61 ± 0.35	SR: 150 rpm T: 25 °C pH: 6 C_0: 5 μg/L Dosage: 10 mg/L	0.5	$q_{e\ calc}$: 0.0145	PSO	SR: 150 T: 25 °C pH: 6 C_0: 5–20 μg/L Dosage: 250 mg/L	K_F: 0.068 (ng/mg)(L/ng)$^{1/n}$	Freundlich	Hydrogen bonding	[213]

Table 6. *Cont.*

Adsorbent Medium	Feedstock	Modification/ Activation	Physico-Chemical Properties	Kinetic Studies				Isotherm Studies			Mechanism	Ref.
				Operational Condition	t_e (h)	q_e (mg/g)/R (%)	Kinetics Model	Operational Condition	Parameter	Isotherms Model		
PAC (F300) Calgon Filtrasorb 300	n.a.	n.a.	n.a.	n.a.	n.a.	n.a.	n.a.	T: 19 °C pH: 7 C_0: 0.1 mg/L Dosage: 0–50 mg/L	Log K_F: 1.2 Log(mg/g)/(L/mg)$^{1/n}$	Freundlich	Polar interactions	[214]
Pristine SCG biochars	Spent coffee grounds	n.a.	S_{BET}: 4.0 m^2/g V_T: 0.006 cm^3/g d: 58.18 Å Ash: 12.6% C: 81.2% H: 1.4% O: 2.2% N: 2.6% H/C: 0.017 O/C: 0.027 N/C: 0.032	SR: 160 rpm T: 25 °C pH: 7 C_0: 1.0 mg/L Dosage: 50 mg/L	24	$q_{e\ calc}$: 1.77	PSO	SR: 160 rpm T: 25 °C pH: 7 C_0: 1.0–10 mg/L Dosage: 50 mg/L t:24 h	1.20 (mg/g)/(L/mg)$^{1/n}$	Freundlich	Pore filling effects Electrostatic interaction Hydrophobic interactions	[215]
Alkali-modified SCG biochars	Spent coffee grounds	Alkaline modification	S_{BET}: 427.5 m^2/g V_T: 0.331 cm^3/g d: 31.13 Å Ash: 15.4% C: 79.7% H: 1% O: 1.8% N: 2.1% H/C: 0.013 O/C: 0.023 N/C: 0.026	SR: 160 rpm T: 25 °C pH: 7 C_0: 1.0 mg/L Dosage: 50 mg/L	720	$q_{e\ calc}$: 19.61	PSO	SR: 160 rpm T: 25 °C pH: 7 C_0: 1.0–10 mg/L Dosage: 50 mg/L t: 24 h	q_m: 91.74 mg/g	Langmuir	Pore filling effects Electrostatic interaction Hydrophobic interactions	[215]
Activated carbon Darco KB-G	n.a.	n.a.	S_{BET}: 364 g/cm^3 V_T: 0.40 cm^3/cm^3 V_{mi}: 0.10 cm^3/cm^3 Λ_{ap}: 0.310 g/mL d: 158 Å	n.a.	n.a.	n.a.	n.a.	T: 25 °C pH: 7 C_0: 250 µg/L Dosage: 1000 mg/L	q_m: 245.10 mg/cm^3	Modified Dubinin–Ashtakov	n.a.	[216]

Table 6. *Cont.*

Adsorbent Medium	Feedstock	Modification/ Activation	Physico-Chemical Properties	Kinetic Studies				Isotherm Studies			Mechanism	Ref.
				Operational Condition	t_e (h)	q_e (mg/g)/R (%)	Kinetics Model	Operational Condition	Parameter	Isotherms Model		
Microsporus carboneus material	Lignocellulose biomass	H_3PO_4	S_{BET}: 1230.6 m^2/g V_{me}: 0.101 cm^3/g V_T: 0.662 cm^3/g V_{mi}: 0.500 cm^3/g C: 64.50% P: 6.33% O: 29.18%	SR: 140 rpm T: 22 $\pm$ 1°C pH: 6–7 C_0: 20 mg/L Dosage: 2000 mg/L	1	$q_{e\,calc}$: 4861 mg/g	PSO	SR: 140 rpm T: 22 $\pm$ 1 °C pH: 6 C_0: 1.0–50 mg/L Dosage: 2000 mg/L t: 1 h	K_F: 5.557 (mg/g) (mg/L)$^{-1/n}$	Freundlich	π–π EDA interaction H bonding	[217]
Activated carbon WVA1110 Mead-Westavaco	Wood-based	Acid activation	S_{BET}: 1648 m^2/g V_{mi}: 0.61 cm^3/g V_{mi}: 0.11 cm^3/g d: <10 Å V_{me}: 0.54 cm^3/g V_T: 1.15 cm^3/g V_{mi}/V_T: 0.53 C: 89.9% N: n.d O: 8.4% S: n.d P: 0.59% Na: 1.08%	SR: 100 rpm T: 30 °C pH: 6.73–7.33 C_0: 100 mg/L Dosage: 500 mg/L	72	n.a.	n.a.	SR: 100 rpm T: 30 °C pH: 6.73–7.33 C_0: 1.0–100 mg/L t: 72 h Dosage: 250 mg/L	q_m: 332.76 mg/g	Sips	n.a.	[169]
Activated carbon S208 Calgon Cargo	Coconuts shells	Physic activation	S_{BET}: 1042 m^2/g V_{mi}: 0.40 cm^3/g V_{mi}: 0.27 cm^3/g d: <10 Å V_{me}: 0.13 cm^3/g V_T: 0.53 cm^3/g V_{mi}/V_T: 0.75 C: 92.6% N: n.d O: 7.4% S: n.d P: n.d Na: n.d	SR: 100 rpm T: 30 °C pH: 6.73–7.33 C_0: 100 mg/L Dosage: 500 mg/L	72	n.a.	n.a.	SR: 100 rpm T: 30 ° C pH: 6.73–7.33 C_0: 1.0–100 mg/L t: 72 h Dosage: 250 mg/L	q_m: 299.72 mg/g	Sips	n.a.	[169]

Table 6. *Cont.*

Adsorbent Medium	Feedstock	Modification/ Activation	Physico-Chemical Properties	Kinetic Studies				Isotherm Studies			Mechanism	Ref.
				Operational Condition	t_e (h)	q_e (mg/g)/R (%)	Kinetics Model	Operational Condition	Parameter	Isotherms Model		
Biochar BC300	pine sawdust	n.a.	S_{BET}: 6.93 m^2/g d: 151.2 Å V_T: 0.02.6 cm^3/g V_{me}: 0.0254 cm^3/g V_{mi}: 6.10^{-5} cm^3/g N: 0.17% C: 72.78% H: 4.56% S: 0.00% O: 20.45% H/C: 0.75 O/C: 0.21	n.a.	n.a.	n.a.	n.a.	T: 25 °C pH: 6 C_0: 0.1–5.0 mg/L Dosage: 25 mg/L t_e: 168 h	q_m: 0.13 mg/g	Sips	n.a.	[218]
Biochar BL300	Pine sawdust	Bleaching treatment	S_{BET}: 14.90 m^2/g d: 75.9 Å V_T: 0.0028 cm^3/g V_{me}: 0.00150 cm^3/g V_{mi}: 0.0013 cm^3/g N: 0.10% C: 28.88% H: 3.54% S: 0.16 O: 25.68 H/C: 1.47 O/C: 0.67	n.a.	n.a.	n.a.	n.a.	T: 25 °C pH: 6 C_0: 0.1–5.0 mg/L Dosage: 25 mg/L t_e: 168 h	q_m: 0.04 mg/g	Sips	n.a.	[218]
Biochar BC500	Pine sawdust		S_{BET}: 151.83 m^2/g d: 33.3 Å V_T: 0.126 cm^3/g V_{me}: 0.05.9 cm^3/g V_{mi}: 0.0731 cm^3/g N: 0.22% C: 80.66% H: 3.08% S: 0.00% O: 11.51% H/C: 0.46 O/C: 0.11	n.a.	n.a.	n.a.	n.a.	T: 25 °C pH: 6 C_0: 0.1–5.0 mg/L Dosage: 25 mg/L t_e: 168 h	q_m: 5.25 mg/g	Sips	n.a.	[218]

Table 6. *Cont.*

Adsorbent Medium	Feedstock	Modification/ Activation	Physico-Chemical Properties	Kinetic Studies				Isotherm Studies			Mechanism	Ref.
				Operational Condition	t_e (h)	q_e (mg/g)/R (%)	Kinetics Model	Operational Condition	Parameter	Isotherms Model		
Biochar BL500	Pine sawdust	Bleaching treatment	S_{BET}: 4.63 m²/g d: 243.5 Å V_T: 0.028 cm³/g V_{me}: 0.0274 cm³/g V_{mi}: 0.0006 cm³/g N: 0.16% C: 67.46% H: 2.89% S: 0.34% O: 17.83% H/C: 0.51 O/C: 0.20	n.a.	n.a.	n.a.	n.a.	T: 25 °C pH: 6 C_0: 0.1–5.0 mg/L Dosage: 25 mg/L t_e: 168 h	q_m: 0.40 mg/g	Sips	n.a.	[218]
Biochar BC700	Pine sawdust		S_{BET}: 353.12 m²/g d: 32.1 Å V_T: 0.284 cm³/g V_{me}: 0.103 cm³/g V_{mi}: 0.182 cm³/g N: 0.13% C: 80.20% H: 1.70% S: 0.08% O: 5.58% H/C: 0.25 O/C: 0.05	n.a.	n.a.	n.a.	n.a.	T: 25 °C pH: 6 C_0: 0.1–5.0 mg/L Dosage: 25 mg/L t_e: 168 h	q_m: 34.59 mg/g	Sips	n.a.	[218]
Biochar BL700	Pine sawdust	Bleaching treatment	S_{BET}: 25.17 m²/g d: 97.5 Å V_T: 0.0610 cm³/g V_{me}: 0.0529 cm³/g V_{mi}: 0.0081 cm³/g N: 0.13% C: 74.28% H: 1.99% S: 0.12% O: 19.77 H/C: 0.32 O/C: 0.20	n.a.	n.a.	n.a.	n.a.	T: 25 °C pH: 6 C_0: 0.1–5.0 mg/L Dosage: 25 mg/L t_e: 168 h	q_m: 0.32 mg/g	Sips	n.a.	[218]

Table 6. *Cont.*

Adsorbent Medium	Feedstock	Modification/ Activation	Physico-Chemical Properties	Kinetic Studies				Isotherm Studies			Mechanism	Ref.
				Operational Condition	t_e (h)	q_e (mg/g)/R (%)	Kinetics Model	Operational Condition	Parameter	Isotherms Model		
Activated carbon	Argan tree nutshells	n.a.	S_{BET}: 1159 m^2/g V_T: 0.64 cm^3/g	n.a.	n.a.	n.a.	n.a.	T: 25 °C C_0: 5.0–50 mg/L Dosage: 100 mg/L t_e: 1 h	K_F: 71.4 (mg/g) (mg/L)$^{-n}$	Freundlich	n.a.	[219]
PAC			S_{BET}: 980 m^2/g d: 19 Å pH$_{pzc}$: 9.5	SR: 150 rpm T: 25 °C pH: 7 C_0: 100 µg/L Dosage: 2000 mg/L	4	$q_{e\ cal}$: 42.20	PSO	SR: 150 rpm T: 25 °C pH: 7 C_0: 40–300 µg/L	K_{HE}: 1.389 L/µg	Linear	Hydrogen bonding Hydrophobic interaction	[220]

Data shown are either reported as such in the articles or calculated with the available data (*). C_0: initial concentration of CBZ (µg/L), d: average pore width (Å), D: average particle size (µm), $IN°$: Iodine number (mg/g), n.a.: not available, pH$_{PZC}$: point of zero charge (-), PSO: pseudo second order, q_e: equilibrium adsorption capacity (mg/g), q_e: calculated equilibrium adsorption capacity (mg/g), q_m: maximum adsorption capacity (mg/g), R: removal efficiency (%), RM: room temperature, t_e: equilibrium time (h), S_{BET}: specific surface area (m^2/g), SR: speed rotation (rpm), V_{me}: mesopore volume (cm^3/g), V_{mi}: microspore volume (cm^3/g), V_T: total pore volume (cm^3/g), $\Lambda_{particle}$: particle density (g/mL), λ_{ap}: apparent density (g/mL).

5.1. Effect of the Adsorbent Properties

5.1.1. Textural Properties

Precursors, pyrolysis temperature and modification or activation processes alter the physico-chemical characteristics of the adsorbent which influence its adsorption capacity [218,221]. Many authors pointed out an increase in the adsorption capacity of the biochar or activated carbon when the S_{BET} and V_{mi} increased.

For instance, Álvarez-Torrellas et al. (2017) studied the removal of CBZ using two different activated carbons, AC-PS and AC-RH, which have been prepared under the same conditions varying only the precursor of the activated carbon. The authors observed a positive correlation between S_{BET} and the adsorption capacity of the activated carbons studied ($S_{\text{BET AC-PS}}$: 1521 m^2/g, $S_{\text{BET AC-RH}}$: 278 m^2/g; q$_{\text{e AC-PS}}$: 241.7 mg/g; q$_{\text{e AC-RH}}$: 170.3 mg/g) [211].

Likewise, Chen et al. (2017) observed that the pyrolysis temperature and acid wash modified the textural properties of biochar and consequently its adsorption capacity. In this study, peanut shells biochar obtained by pyrolysis at 300 °C, 500 °C and 700 °C (BC200, BC300 and BC500, respectively) were modified by HCl washing (HBC200, HBC300 and HBC500, respectively) and with a mixture of HCl/HF washing (FBC200, FBC300 and FBC500, respectively). This study proved that, independently of the modification, the adsorption of CBZ on biochar is enhanced with increasing pyrolytic temperatures. This can be attributed to the enhancement of the S_{BET}, which is a consequence of the transformation of amorphous carbon into aromatic carbon [212].

Among biochars synthesized at the same temperature, the authors noticed that those produced at 500 °C presented a higher $V_{T,}$ after acidic washing, while at 300 °C and 200 °C this effect was not observed. This may be due to the pore structures being not well developed in BC200 and BC300 so that the acid-wash treatment was unable to enhance their S_{BET} [212]. Similarly, Chu et al. (2019) pointed out that by increasing the pyrolytic temperature of biochar, the S_{BET} and V_{mi} increased and, as a consequence, the adsorption capacity [218].

Another study conducted by Shin et al. (2020) demonstrated that the alkali modification of SCG biochar (Spent Coffee Grounds biochar) enhanced its textural properties (alkali-modified SCG biochar: S_{BET}: 427.5 m^2/g and V_T: 0.333 cm^3/g; SCG biochar: S_{BET}: 4.0 m^2/g, V_T: 0.006 cm^3/g). The enhancement of the S_{BET} and V_T was associated with an improvement of adsorption capacities (SCG biochars q_e: 1.72 mg/g and alkali-modified SCG biochars q_e: 19.77 mg/g) [215].

Furthermore, Nielsen et al. (2014) demonstrated that the increment of textural properties for two commercially activated carbons, WVA1110 (a wood-based carbon) and S208 (obtained from coconut shells), enhanced the adsorption capacity [169]. WVA1110 activated carbon presented higher S_{BET} and V_{mi} than S208 activated carbon (i.e., 60% and 50% higher, respectively). However, S208 activated carbon presented more pores smaller than <10 Å as compared to WVA1110 activated carbon, which signifies that S208 activated carbon predominated physical interaction with CBZ, while WVA1110 activated carbon chemical interaction. Therefore, the interaction between CBZ and WVA1110 was proved to be specific and the adsorption capacity of WVA1110 was higher than that of S208 [169].

El Mouchtari et al. (2020) compared an activated carbon with the same activated carbon modified with 9% TiO [219]. They noticed that modified activated carbon presented a smaller maximum adsorption capacity than activated carbon without any modification. This reduction of the maximum adsorption capacity was associated with the drastic decrease in its S_{BET} (activated carbon: S_{BET}: 1159 m^2/g, V_T: 0.64 cm^3/g, q_m: 175.4 mg/g; activated carbon 9% TiO: S_{BET}: 9.59 m^2/g V_T: 0.52 cm^3/g, q_m: 153.8 mg/g) [219].

5.1.2. Chemical Surface

Chemical properties such as elemental compositions, functional groups, bulk polarity and ash content, influence the adsorption capacity of biochar and activated carbon. For instance, Torrellas Álvarez et al. (2015) studied the removal of the CBZ using activated

carbon (PS), a thermic treated activated carbon (He-PS) and an activated carbon treated with HNO_3 (O-PS). They pointed out that the modification did not considerably affect the textural properties but altered the chemical properties like the type of functional groups and their concentration. Furthermore, O-PS presented an important increase in the concentration of the oxygenated surface groups compared to PS due to the oxidation with HNO_3. The enhancement of the oxygenated surface groups made O-PS less hydrophobic and less affine to CBZ compared with PS ($q_{m\ PC}$: 14234 mg/g $q_{m\ O-PC}$: 2456 mg/g). This decrease was explained due to the competitive effect between CBZ and water molecules for the available activated sites [182].

Pyrolysis temperature and acidic modification also alter chemicals properties. For example, Chen et al. (2017) pointed out that pyrolysis temperature and acid wash also modified the chemical surface properties of biochars. They analyzed the data from adsorption studies by Dubin–Ashtakhov kinetic model which described fast and slow adsorption of CBZ. It was noticed that fast and slow adsorption were affected by varying the carbon structure. At higher pyrolysis temperature, fast adsorption was favored because of the higher aromatic carbon component, while at lower pyrolysis temperature, slow adsorption was enhanced because of higher amorphous carbon component. The increment of the aromatic carbon component with the increased temperature is justified by the decreasing H/C ratio. On the other hand, at the same pyrolysis temperature, acid-washed biochar (FBC and HBC) presented a minor CBZ adsorption capacity than biochar (BC). This may be attributed to the decrease of the ash content due to the acid washing [212].

Likewise, Chu et al. (2019) noticed that the adsorption capacity of biochar increased when the biochar pyrolytic temperature increased, due to the enhancement of condensed aromatic carbons since biochar obtained at higher temperatures presented higher O% content H/C and O/C ratios while less C% content. On the other hand, after bleaching treatment, the adsorption capacity of the biochars decreased because of the removal of noncondensed aromatic carbons. This is probably related to the increasing H/C [218].

According to Shin et al. (2020), the alkali-modified SCG biochar presented smaller elemental content (C, H, N, O) and lower values of the H/C O/C and N/C ratios than SCG biochar. These results indicated that the alkali-modified SCG biochars were more carbonized than the SCG biochars. Furthermore, alkali-modified SCG biochar presented only a strong infrared (IR) peak associated with carboxylic acids (C = O) while SCG biochar presented two IR peaks, one associated with carboxylic acids (C = O) and the other one associated with ether (C-O-C). These differences made alkali modified SCG biochar more hydrophobic than SCG biochar, leading to its higher affinity and higher CBZ removal [215].

5.1.3. Effect of the Log K_{ow}

Octanol/water partition coefficients (Log K_{ow}) of organic pollutants represent their hydrophobicity character. Thus, higher K_{ow} indicates higher hydrophobicity character and higher affinity of a substance to the adsorbent [211].

However, it is important to consider other factors that can affect adsorbability. For instance, Yu et al. (2008) noticed that among three compounds adsorbed onto activated carbon, nonylphenol (Log K_{ow}: 5.8), naproxen (log K_{ow}: 3.18) and CBZ (Log K_{ow}: 2.45), nonylphenol was the less adsorbed onto two activated carbons, the second one was naproxen while the most adsorbed was CBZ, which was the opposite to what had been expected according to their Log K_{ow}. The lower adsorption affinity of naproxen compared to CBZ can be explained by the dissociation of the acidic naproxen at experimental pH. If naproxen Log K_{ow} is recalculated according to Equation (23) for acid compounds so that modified Naproxen Log K_{ow} becomes lower than CBZ Log K_{ow}, its lower affinity to the activated carbons concerning CBZ becomes evident.

However, the lowest affinity of nonylphenol, which is a neutral compound at water pH, to the activated carbon could be due to the strong bonding between nonylphenol hydrophilic group and activated carbon when the nonylphenol concentration is low, but at high concentration, the mechanism was not clear [45].

In another study of the same research group, Yu et al. (2005) found the same tendency: nonylphenol presented lower adsorption capacity than naproxen and CBZ, even if nonylphenol had a higher Log K_{ow} than the other two compounds. They postulated that the adsorption also depends on other properties such as functional groups and surface charge of adsorbents [209].

Furthermore, Álvarez-Torrellas et al. (2017) noticed that CBZ and ciprofloxacin presented similar adsorptive affinity towards the carbon surface even if CBZ has a higher Log K_{ow} than ciprofloxacin. According to the authors, this effect could be mainly attributed to strong π-π electron Donor−Acceptor [211]:

$$K'_{ow} : \frac{K_{ow}}{1 + 10^{(pH-pKa)}} \tag{23}$$

where K'_{ow} represents the K_{ow} corrected based on the experimental pH, for neutral species and pK_a is the negative base-10 logarithm of the acid dissociation constant (K_a).

According to the studies above presented, the Log K_{ow} of CBZ can help to predict how this one will behave in the adsorption process; however, the pH of the water solution or the interaction between the molecule and the surface of the carbon material can cause a relevant difference between the predicted and the observed behavior.

5.2. Effect of Operational Conditions

5.2.1. pH

pH is an important factor that affects the adsorption of CBZ since it can modify the surface charge of the adsorbent and the speciation of the molecule (see Table 7) [186,201].

Table 7. Effect of pH on carbamazepine adsorption.

Adsorbent Medium	Operational Condition	Modified Parameter	R/q_m (mg/g)	Ref.
Activated carbon PKS	SR: 250 rpm T: 25 °C C_0: 250 mg/L Dosage: 1000 mg/L t: 24 h	pH: 3 5 10	R (%): 80 80 80	[201]
Mesoporous activated carbon (Meso-AC 1)	T: 25 ± 2 °C C_0: 50 mg/L Dosage: 100 mg/L t: 0.5 h	pH: 2 4 6 8 10	q_m (mg/g): 113 165 170 188 140	[186]
Pristine SCG biochars	SR: 160 rpm T: 25 °C C_0: 1.0 mg/L Dosage: 50 mg/L t: 24 h	pH: 3 7 11	R (%): 10 10 10	[215]
Alkali-modified SCG biochars	SR: 160 rpm T: 25 °C C_0: 1.0 mg/L Dosage: 50 mg/L	pH: 3 7 11	R (%): 100 100 100	[215]

Data shown are either reported as such in the articles or calculated with the available data. C_0: initial concentration of CBZ (µg/L), q_m: maximum adsorption capacity (mg/g), R: removal efficiency (%), SR: speed rotation (rpm), t: time (h), T: temperature (°C).

CBZ presents two pK_a values, i.e., 2.3 and 13.9 and in this range is into zwitterion forms; below pH 2.3, CBZ is positively charged, while above pH 13.9 it is negatively charged [45,201,222]. Table 7 summarizes the results of some studies in which the CBZ adsorption test was conducted at different pH and temperature values.

For instance, To et al. (2017) observed that at pH 3, 5 and 10, the adsorption removal of CBZ from water solution by PKS activated carbon was the same, concluding that since

in this pH range CBZ was uncharged the adsorption process involves hydrophobic and π-π bonding [201].

Similarly, Shin et al. (2020) noticed that the adsorption removal of CBZ onto SCG biochar and alkali-modified SCG biochar did not change with the variation of the pH in the range 3–11 [215]. On the other hand, Ncibi and Sillanpää (2017) showed that adsorption capacity of CBZ onto mesoporous activated carbon (Meso-AC 1) increased into pH range 2–8 (from 113 mg/g to 188 mg/g) while from pH 8 to 10 the adsorption capacity decreased from 188 mg/g to 140 mg/g approximately. According to the authors, this change in the adsorption capacity could be due to a combination of mechanisms such us hydrophobic and π-π interaction between CBZ's benzene ring and the activated carbon [186].

Likewise, Naghdi et al. (2017) also observed an increase of CBZ removal when the pH increases from 3 to 9. According to the authors, this tendency may be explained by the presence of cations H^+ in the medium [213].

Thus, at lower pH there is a higher H^+ concentration so the functional group of CBZ could interact more easily with the H^+ present in the medium, while at higher pH, where H^+ concentration is lower, the hydrogen bonding donor groups on CBZ could interact with hydrogen bonding acceptors or π donor into adsorbent material, thus enhancing the removal capacity [213].

Suriyanon et al. (2013) did not show any consistent relationship between pH change and CBZ adsorption capacity onto PAC, which may be due to the various types of surface functional groups onto the PAC surface [220].

5.2.2. Temperature

Temperature can also influence CBZ adsorption, as shown in Figure 1. Ncibi and Sillanpää (2017) noticed that CBZ removal efficiency onto activated carbon (Meso-AC1) increased from 104 to 251 mg/g for temperature solution increase from 15 to 45 °C, respectively [186].
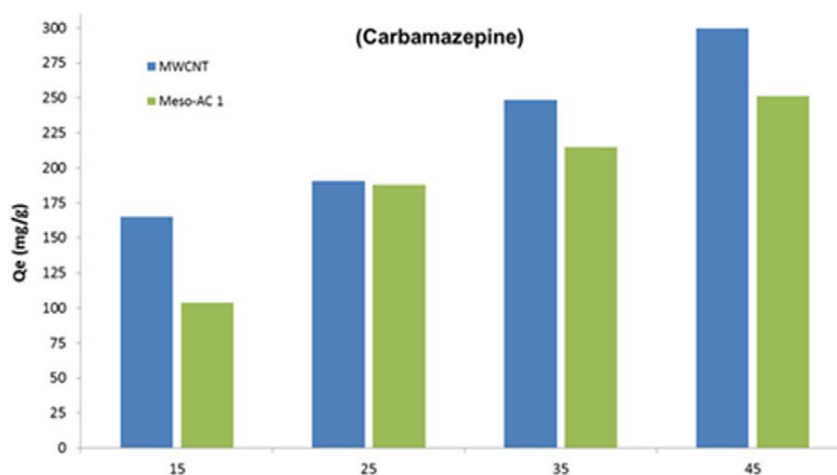
Figure 1. Influence of temperature on CBZ removal by Meso-AC1 and MWCNT [186]. Reprinted from Journal of Molecular Liquids, 238, Mohamed Chaker Ncibi,Mika Sillanpää, Optimizing the removal of pharmaceutical drugs Carbamazepine and Dorzolamide from aqueous solutions using mesoporous activated carbons and multi-walled carbon nanotubes 379-388 Copyright (2017), with permission from Elsevier.

This result is in agreement with the study conducted by Suriyanon et al. (2013) in which the variation of the CBZ adsorption onto PAC with the temperature change was related to the Gibbs free energies. The authors concluded that the Gibbs free energies of the adsorption (DGo) increased when temperature increased, thus suggesting that the adsorption is more favorable at higher temperatures [220].

5.2.3. Rotational Speed

The rotational speed of the batch tests can also influence CBZ adsorption. Naghdi et al. (2017) studied how CBZ adsorption changed whit the rotational speed in the adsorption process. They concluded that CBZ adsorption enhanced from 29% to 67% with the increase of the rotational speed from 90 to 210 rpm, while from 210 to 240 rpm any considerable increment was observed [213].

These results are in accordance with Walker et al. (2003) who suggested that, around the adsorbent, there is a thin layer where the surface viscous forces resist against fluid movement, impeding mass transfer of the adsorbate. Thus, higher rotational speed causes a higher mass transfer and consequently a higher adsorption [213,223].

5.2.4. Presence of Competitive Contaminants

In water and wastewater, CBZ is usually present with other contaminants so it is important to study CBZ adsorption in multicomponent solutions. However, little research has compared single CBZ adsorption with competitive CBZ adsorption.

The few available data sets highlighted a reduction in the CBZ adsorption due to the competitive effect (see Table 8).

For instance, Álvarez-Torrellas et al. (2017) noticed a reduction in CBZ adsorption in bi-component solution (CBZ 100 mg/L and ciprofloxacin hydrochloride (CPX) 100 mg/L) concerning CBZ in a single solute solution. They postulated that this difference can be related to the textural properties of the adsorbent. A high affinity of CBZ was observed towards AC-F400 and as a consequence, a reduction of the adsorption capacity was observed for CPX (of 67% and 80% for CBZ and CPX, respectively, between single and binary solutions) which can be explained by the minor molecular weight of CBZ with respect to CPX. Thus, CBZ can easily arrive at the inner microporous surface of AC-F400 activated carbon [211]. The same tendency was observed by Suriyanon et al. (2013): the adsorption capacities of PAC for CBZ decreased when CBZ was in a binary solution with diclofenac, which can be due to the complexity of the functional groups on PAC surface and the disorder of its microporous structure [220].

Similarly, Shin et al. (2020) noticed that on the alkali-modified SCG biochars there was a reduction of the CBZ adsorption equal to 61% when the adsorption was carried out in a multicomponent solution (i.e., CBZ, 17 α-ethinylestradiol, Ibuprofen). In contrast, when CBZ adsorption from a single solution was carried out onto SCG biochars (not modified), CBZ removal was similarly close to multicomponent solution adsorption. Furthermore, the CBZ removal from multicomponent solution was not affected by pH changes and was the same as removal from single solution [215].

Delgado et al. (2019) also studied the competitive effect in CBZ adsorption and noticed that at higher initial concentrations ($C_0 \approx 5.0$ mg/L), the adsorption kinetics of CBZ was slower in multicomponent solution (CBZ and sildenafil citrate) than in CBZ single solution. However, at a small initial concentration (200 μg/L), there were no significate differences between CBZ adsorption from multicomponent solution and single solution [159].

Table 8. Comparison of CBZ adsorption between single and multicomponent solutions.

Adsorbent Medium	Operational Condition	Single CBZ Solution	Multicomponent CBZ Solution		Ref.
		R/Adsorption Parameter	Composition	R/Adsorption Parameter	
Activated carbon Calgon Filtrasorb 400	SR: 250 rpm T: 30 °C t_e: 4 h pH: 6.5 C_0: 100 mg/L Dosages: different	$q_{e\,exp}$: 220.2 mg/g	CBZ Ciprofloxacin hydrochloride C_0 of each component: 100 mg/L	$q_{e\,exp}$: 71.5 mg/g % decreasing: 67.5	[211]
Activated carbon (AC-PS)	SR: 250 rpm T: 30 °C t_{eq}: 4 h pH: 6.5 C_0: 100 mg/L Dosages: different	$q_{e\,exp}$: 241.7 mg/g	CBZ Ciprofloxacin hydrochloride C_0 of each component: 100 mg/L	$q_{e\,exp}$: 129.2 mg/g % decreasing: 46.5	[211]
Activated carbon AC-RH	SR: 250 rpm T: 30 °C t_e: 4 h pH: 6.5 C_0: 100 mg/L Dosages: different	$q_{e\,exp}$: 170.3 mg/g	CBZ Ciprofloxacin hydrochloride C_0 of each component: 100 mg/L	$q_{e\,exp}$: 73.5 mg/g % decreasing: 56.8	[211]
PAC Biopack	SR: 90 rpm T: 25 °C pH: 6.15 t: 10 h Dosage: 100 mg/L C_0: 4500 ± 200 µg/L	R: 10%	CBZ: C_0 4.5 ± 0.2 mg/L Sildenafil citrate: C_0 5.100 ± 1 mg/L	R: 40%	[159]
PAC Biopack	SR: 90 rpm T: 25 °C pH: 6.15 t: 10 h Dosage: 100 mg/L C_0: 130 ± 10 µg/L	R: 10%	CBZ: C_0 130 ± 10 µg/L Sildenafil citrate C_0: 0.210 ± 0.050 mg/L	R: 10%	[159]
Pristine SCG biochars	SR: 160 rpm T: 25 °C pH: 7 t_e: 24 h C_0: 1.0 mg/L Dosage: 50 mg/L	q_e: 1.77 mg/g (PSO) K_F: 1.20 $(mg/mg)(L/mg)^{1/n}$	CBZ 17 α-ethinylestradiol Ibuprofen C_0 of each component: 1.0 mg/L	q_e: 1.76 mg/g (PSO) K_F: 2.58 $(mg/mg)(L/mg)^{1/n}$	[215]
Alkali-modified SCG biochars	SR: 160 rpm T: 25 °C pH: 7 t_e: 24 h 1.0 mg/L Dosage: 50 mg/L	q_e: 19.61 mg/g q_m: 91.74 mg/g	CBZ 17 α-ethinylestradiol Ibuprofen C_0 of each component: 1.0 mg/L	q_e: 18.76 mg/g q_m: 30.40 mg/g	[215]
Pristine SCG biochars	SR: 160 rpm T: 25 °C t: 24 h C_0: 1.0 mg/L Dosage: 50 mg/L pH 3 7 10	R (%): 10% 10% 10%	CBZ 17 α-ethinylestradiol Ibuprofen C_0 of each component: 1.0 mg/L	R (%): 10% 10% 10%	[215]
Alkali-modified SCG biochars	SR: 160 rpm T: 25 °C t: 24 h C_0: 1.0 mg/L Dosage: 50 mg/L pH 3 7 10	R (%): 90 90 90	CBZ 17 α-ethinylestradiol Ibuprofen C_0 of each component: 1.0 mg/L	R (%): 90 90 90	[215]

Data shown are either reported as such in the articles or calculated with the available data. C_0: initial concentration of CBZ (µg/L), K_F: Freundlich constant $[(mg/mg)(L/mg)^{1/n}]$, $q_{e\,exp}$: experimental equilibrium adsorption capacity (mg/g), q_e: equilibrium adsorption capacity (mg/g), R: Removal efficiency (%), SR: Speed rotation (rpm), t: time (h), t_e: equilibrium time (h), T: temperature (°C).

5.2.5. Organic Matter

Table 9 summarizes some of the studies in which CBZ adsorption was compared in the absence and presence of dissolved organic matter (DOM).

Table 9. Comparison of CBZ adsorption in the presence and absence of DOM.

Adsorbent Medium	Operational Condition	CBZ Solution without DOM	CBZ Solution with DOM		Ref.
		R/Adsortion Parameter	Characteristics/ Composition	R/Adsortion Parameter	
PAC Biopack	SR: 90 rpm T: 25 °C pH: 6.15 t: 10 h Dosage: 100 mg/L C_0: 130 ± 10 μg/L	R: 10%	WW from a secondary treatment pH: 7.3–7.5 DO: 4.7–5.3 mg/L T: 19.2–21.5 °C Conductivity: 0.96–1.03 ms/cm COD: 18–27 mg/L	R: 10%	[159]
PAC (F300) Calgon Filtrasorb 300	T: 19 °C pH: 7 t_e: 1440 C_0: 100 μg/L Dosage (mg/L): 0.5 1.0 3.0 5.0 10.0 20.0 50.0	R (%): 0 10 20 37 75 100 100 Log K_F: 1.2 $(mg/g)/(L/mg)^{1/n}$	Effluent organic matter (EfOM) Total organic carbon 4.0 mg/L	R (%): 0 10 20 37 55 70 75 Log K_F: 2.6 $(mg/g)/(L/mg)^{1/n}$	[214]
Pristine SCG biochars	SR: 160 rpm T: 25 °C pH: 7 t: 1440 min C_0: 1.0 mg/L Dosage: 50 mg/L	R: 9.6%	Humic acids: 5.0 mg/L	R: 2.5%	[215]
Alkali-modified SCG biochars	SR: 160 rpm T: 25 °C t: 1440 min pH: 7 C_0: 1.0 mg/L Dosage: 50 mg/L	R: 95.9%	Humic acids: 5.0 mg/L	R: 94.1%	[215]
Pristine SCG biochars	SR: 160 T: 25 °C pH: 7 t: 24 h C_0: 1.0 mg/L Dosage: 50 mg/L	R: 8.7%	Humic acids: 5.0 mg/L 17 α-ethinylestradiol: 1.0 mg/L Ibuprofen: 1.0 mg/L	R: 6.6%	[215]
Alkali-modified SCG biochars	SR: 160 rpm T: 25 °C t: 24 h pH: 7 C_0: 1.0 mg/L Dosage: 50 mg/L	R: 82.3%	Humic acids: 5 mg/L 17 α-ethinylestradiol: 1.0 mg/L Ibuprofen: 1.0 mg/L	R: 75.3%	[215]
GAC PICACTIF TE (PICA)	SR: 120 rpm T: 23 ± 1 °C C_0: 1 μg/L Dosage: 1–10 mg/L t: 288 h	K_F: 57.56 $(ng/mg)(L/ng)^{1/n}$	Post sedimentation water sterilized from a full-scale WTPs DOC: 3.0–5.4 mg/L pH: 7.5–7.9	K_F: 4.53 $(mg/g)(L/mg)^{1/n}$	[45]
GAC Calgon Filtrasorb 400 (F400)	SR: 120 rpm T: 23 ± 1 °C C_0: 1 μg/L Dosage: 1–10 mg/L t: 288 h	K_F: 73.79 $(ng/mg)(L/ng)^{1/n}$	Post sedimentation water sterilized from a full-scale WTPs DOC: 3.0–5.4 mg/L pH: 7.5–7.9	K_F: 2.82 (mg/g) $(L/mg)^{1/n}$	[45]

Data shown are either reported as such in the articles or calculated with the available data. C_0: initial concentration of carbamazepine (μg/L or mg/L), DO: dissolved oxygen (mg/L), DOC: dissolved organic carbon (mg/L), K_F: Freundlich constant $[(mg/mg)(L/mg)^{1/n}]$, q_e: equilibrium adsorption capacity (mg/g), R: Removal efficient (%), SR: Speed rotation (rpm), t: time (h or min), T: temperature (°C).

For instance, Shin et al. (2020) studied single and competitive CBZ adsorption (CBZ, 17 α-ethinylestradiol, ibuprofen, C_0: 1 mg/L) with and without DOM (C_0: 5 mg/L) onto the pristine and alkali-modified SCG biochars. It was shown that the CBZ removal in presence of DOM was less than that in absence of DOM either in the CBZ single or the competitive adsorption (SCG biochars: single removal efficiency of CBZ without DOM: 9.6%; single removal efficiency of CBZ with DOM: 2.5%; competitive removal efficiency of CBZ without DOM: 8.7%; removal efficiency of CBZ with DOM: 6.6%; Alkali-modified SCG biochars: single removal efficiency of CBZ without DOM: 95.9%; single removal efficiency of CBZ with DOM: 94.1%). They concluded that DOM competes with CBZ for the activated sites, causing a decrease in CBZ adsorption, since the hydrophobic interactions between DOM and the adsorbent surfaces negatively affect the adsorption of CBZ [215].

Similarly, Yu et al. (2008) studied CBZ adsorption from ultrapure water and from postsedimental wastewater (PS) at a spiked concentration of 1.0 mg/L. They noticed a competition between CBZ and DOM based on the reduction of the K_F. The authors suggested that the competition between CBZ and DOM can be attributed to the similar size of a part of the DOM and CBZ molecules [45].

Furthermore, Dickenson and Drewes (2010) compared the CBZ adsorption in ultrapure water and in Effluent Organic Matter aqueous matrices (EfOm) using different activated PAC dosages. They noticed that at higher PAC dosages (>10 mg/L), CBZ adsorption in EfOm was less than that in ultrapure water, while at lower PAC dosages (<10 mg/L) it did not differ in the two matrices [214].

On the other hand, according to Delgado et al. (2019), no significant differences in CBZ adsorption were observed using ultrapure water or wastewater [159].

5.3. Adsorption Mechanisms

Different mechanisms have been proposed to explain the CBZ adsorption onto activated carbon and biochar, as shown in Figure 2.
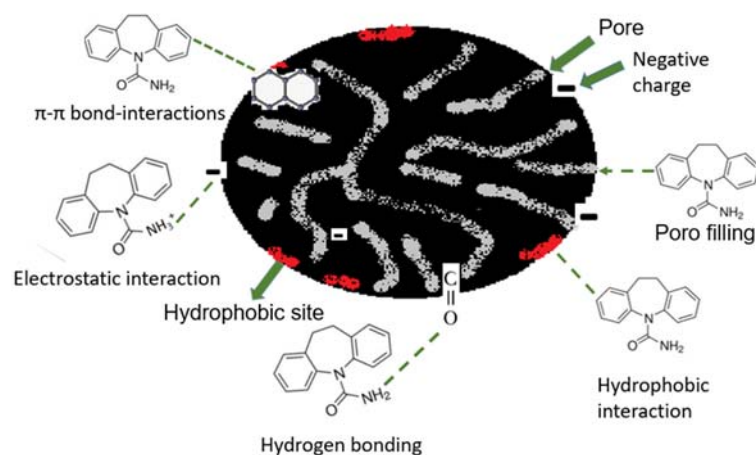
Figure 2. CBZ adsorption mechanisms onto activated carbon and biochar.

One of them is the pore-filling mechanism, which is the main mechanism involved in the adsorption of small-size organic compounds such as CBZ [224]. This mechanism explains why the CBZ adsorption onto two different activated carbons (such as AC-PS and AC-RH) was positively correlated with S_{BET} [224].

Other mechanisms suggested are hydrophobic interaction and π-π interaction: Chen et al. (2017) highlighted that π-π interaction might be an important mechanism of the CBZ adsorption onto biochar (BC, HBC and FBC series) due to a significant negative correlation between K_d (solid–liquid partition coefficient) and (O + N)/C and K_d and H/C [212].

Similar interactions were proposed by To et al. (2017) and Ncibi and Sillanpää (2017) who affirmed that no electrostatic interaction occurred between CBZ and activated carbon

because in the pH range of the adsorption process CBZ is a neutral molecule (pK$_{a1}$: 2.3 and pK$_{a2}$: 13.9) [186,201].

Likewise, Shin et al. (2020) noticed that the adsorption removal order of 17α-ethinyl estradiol (EE2), ibuprofen and CBZ agreed with the order of the Log D (distribution coefficient) values of the micropollutants under different pH conditions. Thus, the authors concluded that pore-filling, electrostatic and hydrophobic effects were the main interactions in the removal of CBZ by the studied biochars [215].

5.4. Kinetic and Isotherm Models of CBZ Adsorption onto Carbon-Based Sorbents

5.4.1. Adsorption Kinetics Models

The adsorption kinetics studies are important because they provide information about the rate of the adsorption process and point out the main factors that affect the rate of reaction [221]. The adsorption process involves three steps: external mass transfer, internal diffusion, and adsorption. During the external mass transfer, the adsorbate moves from the solution to the external surface of the adsorbent; in the internal diffusion, the adsorbate migrates to the sorption sites and finally, during the adsorption the adsorbate is linked to the adsorbent [225]. To study the different mechanisms of adsorption, many kinetics models have been developed. Kinetics models, such as pseudo-first-order, pseudo-second-order, Elovich, Pseudo n order, consider the adsorption as the limiting step. On the other hand, models like Weber and Morris, Crank and Boyd suppose that the diffusion process is the limiting step [221,226]. Nonlinear regression and/or linear regression can be applied for calculating kinetic parameters. Following the kinetics models identified in the CBZ adsorption studies are described.

Pseudo-First-Order

The pseudo-first-order (PFO) model, initially proposed by Lagergren [227] is based on a nonreversible reaction where the rate of adsorption over time is directly proportional to the number of unoccupied sites by the adsorbate [159,228]. The PFO model can be expressed as the nonlinear Equation (24):

$$q_t = q_e \left(1 - e^{k_1 t}\right) \tag{24}$$

where k_1 is the apparent rate constant (L/min), q_t and q_e (mg/g) are the adsorption capacity at time t and at equilibrium. Its linearized form is also presented below:

$$\ln(q_e - q_t) = q_e - k_1 t \tag{25}$$

Pseudo Second Order

The pseudo-second-order (PSO) model, proposed by Ho and McKay [229], is based on the assumption that the limiting phase is the chemical adsorption. The adsorption rate, over the entire adsorption process, is considered proportional to the square of the number of unoccupied sites [230]. In this condition, the adsorption rate does not depend on the equilibrium concentration, but on the adsorption capacity [231]. The PSO model equation can be expressed in the nonlinear Equation (26) below [232]:

$$q_t = \frac{k_2 q_e^2}{1 + k_2 q_e t} \tag{26}$$

where k_2 is the apparent rate constant [g/(mg min)] [233]; its linearized form is also presented below:

$$\frac{t}{q_t} = \frac{1}{k_2 q_e^2} + \frac{1}{q_e} t \tag{27}$$

Two-Compartment First-Order Adsorption Model

A two-compartment first-order adsorption model (2-CFOSM) describes the adsorption kinetics on carbon-based sorbents to reveal the effects of varying the carbon structure and mineral composition of carbonaceous material on fast and slow adsorption. The 2-CFOSM model equation is described below [212]:

$$\frac{q_t}{q_e} = f_f\left(1 - e^{-k_s t}\right) + f_s\left(1 - e^{-k_f t}\right) \tag{28}$$

f_f, f_s and k_f, k_s represent the fractions (-) and the rate constants (1/h) of the two compartments (f = fast and s = slow), respectively.

Ritchie Second-Order and Modified Ritchie Second-Order

Ritchie (1977) [234] used a second-order empirical equation to represent the kinetic adsorption of gases onto a solid; afterwards, it has also been applied to solid/solution sorption systems [235]. The Ritchie second-order and modified second-order models are usually used to measure the initial particle loading [201,208].

The Ritchie second-order [208] model equation can be expressed as in Equation (29):

$$q_t = q_e\left[1 - \left(\frac{1}{1 + k_R t}\right)\right] \tag{29}$$

where k_R represents the Ritchie second-order rate constant (L/min).

The modified Ritchie second-order [201] model equation can be expressed as in Equation (30):

$$q_t = q_e\left[1 - \left(\frac{1}{\beta_2 + k_{mR} t}\right)\right] \tag{30}$$

where β_2 and k_{mR} represent the surface coverage of the adsorbent (or the initial particle loading) and the modified Ritchie second-order rate constant (L/min), respectively [208].

Diffusion-Chemisorption

The diffusion-chemisorption model was developed to simulate sorption of heavy metals unto heterogeneous media, through an empirical differential equation proposed by Sutherland (2004) [236]. This model is described by the nonlinear Equation (31):

$$q_t = \frac{q_e K_{CD} t^{0.5}}{k_{DC} + q_e} \tag{31}$$

It can be expressed linearly as Equation (32):

$$\frac{t^{0.5}}{q_t} = \frac{1}{k_{DC}} + \frac{1}{q_e} t^{0.5} \tag{32}$$

where k_{DC} is the diffusion-chemisorption constant [mg/(g h$^{0.5}$)] [237,238].

5.4.2. Adsorption Isotherms Models

Equilibrium sorption isotherms studies are useful to determine the adsorption capacity of the adsorbent for an adsorbate [239]. Thus, many adsorption isotherms models, such as Freundlich, Langmuir, Redlich–Peterson, Linear, etc., have been studied [240,241].

Nonlinear regression and/or linear regression can be applied for calculating isotherm parameters. Next, the isotherm models identified in the CBZ adsorption studies are described.

Linear

The linear, or Henry's isotherm model, is considered the simplest adsorption isotherm model [242]. The relationship between concentration and adsorption capacity, at equilibrium time, can be expressed linearly as the Equation (33) [220]:

$$q_e = K_{HE}C_e \tag{33}$$

where K_{HE} is the linear constant (L/g) [243]. To determine the Henry maximum adsorption capacity (q_m), it is necessary to pose the concentration equal to the value at the beginning ($t = 0$):

$$q_m = K_{HE}C_0 \tag{34}$$

Langmuir

The Langmuir adsorption isotherm was the first to be used to describe the gas–solid-phase adsorption [244].

In the reversible monolayer adsorption of the Langmuir model, the adsorbent and the adsorbate are in dynamic equilibrium through a homogeneous surface coverage of the adsorbate molecules on the adsorbent, expressed as fractional coverage and depending on the equilibrium concentration of the adsorbate [240]. This model is represented as follows in the nonlinear form [245]:

$$q_e = \frac{q_m K_L C_e}{1 + K_L C_e} \tag{35}$$

where q_m is the maximum amount of adsorbate per unit of adsorbent mass (mg/g) and K_L is the Langmuir equilibrium constant (L/ng) related to the adsorption capacity and energy of adsorption [232].

Freundlich

Freundlich isotherm describes a multilayer reversible adsorption at a heterogeneous surface through an exponential nonlinear equation [246]. The model assumes that the adsorption capacity increases with the adsorbate concentration [36]. The expression of the Freundlich equation is given as Equation (36) [202]:

$$q_e = K_F C_e^{\frac{1}{n}} \tag{36}$$

where K_F is the adsorption affinity-related parameter [(mg/kg) (mg/L)$^{1/n}$] and n is the nonlinear coefficient.

To determine the Freundlich maximum adsorption capacity (q_m), once the Freundlich parameters have been calculated, it is necessary to insert the initial constant concentration in Equation (35), instead of that of equilibrium, thus, according to Halsey [247]:

$$q_m = K_F C_0^{\frac{1}{n}} \tag{37}$$

Redlich–Peterson

The Redlich–Peterson model is a combination of the Langmuir and Freundlich approaches and it may be used to represent the dependence of adsorption capacity over a wide concentration range [245]. The nonlinear form of this three-parameter empirical model is given in Equation (38):

$$q_e = \frac{K_{RP}C_e}{1 + a_{RP}C_e^{n_{RP}}} \tag{38}$$

where K_{RP} (L/g), a_{RP} [(mg/L)-$^{n_{RP}}$] and n_{RP} (-) are the Redlich–Peterson constants; n_{RP} ranges between 0 and 1. The Redlich–Peterson maximum adsorption capacity can be calculated using Equation (39) [248]:

$$q_m = \frac{K_{RP}}{a_{RP}} \tag{39}$$

Sips

The Sips isotherm, also known as the Freundlich–Langmuir model, is a combination of the Freundlich and Langmuir models; in fact, it has a form similar to Freundlich isotherm, differing in the maximum adsorption capacity at a sufficiently high concentration [249]. Therefore, this model is suitable for predicting adsorption on heterogeneous surfaces, as the increase of adsorption capacity is limited, normally associated with the Freundlich model [242]. Its nonlinear form equation can be represented as follows:

$$q_e = q_m \frac{K_S C_e^{n_S}}{1 + K_S C_e^{n_S}} \tag{40}$$

where q_m is the maximum adsorption capacity (mg/g); K_S (L/g) and n_S (-) represent the affinity constant for the adsorption and the index of heterogeneity which can vary from 0 to 1, respectively [248,250].

Guggenheim–Anderson–De Boer

Guggenheim–Anderson–De Boer (GAB) model considers multilayer adsorption by assuming that each molecule in the first adsorbed layer provides one site for the second and subsequent layer [251,252]. The GAB equation is defined by the following nonlinear Equation (41) [211]:

$$q_e = \frac{q_{m,1} K_1 C_e}{(1 - K_2 C_e)[1 + C_e(K_1 - K_2)]} \tag{41}$$

where K_1 and K_2 (L/mg) are the equilibrium constants for the first and the second layer, respectively; $q_{m,1}$ (mg/g) is the maximum adsorption capacity on the first layer.

Dubinin–Ashtakhov

Dubinin–Ashtakhov (DA) model considers the mathematical formulations of the Polanyi theory and Weibull statistic distribution [253], to obtain a thermodynamic model for adsorption. Nonlinear equation of DA model is presented by Equation (42) [254]:

$$q_e = q_m \exp\left[-\left(\frac{\theta}{E}\right)^b\right] \tag{42}$$

where E and b are the adsorption energy (kJ) and the surface heterogeneity, respectively, θ (kJ/mol) is the adsorption potential as defined by Equation (43):

$$\theta = R_{GAS} T \ln\left(\frac{C_S}{C_e}\right) \tag{43}$$

where R_{GAS} is the universal gas constant, equal to 8.314×10^{-3} kJ/(mol °K), T is the absolute temperature (°K) and C_s (mg/L) is the adsorbate solubility in the solvent used [255].

The modified Dubinin–Ashtakov (MDA) model is presented below in the nonlinear form (43), which takes into account the difference between the contaminant adsorbed on the carbonaceous material and the amount that would be present in the same volume, at the same temperature and pressure, in the absence of adsorption [256]:

$$q_{e,mod} = q_m \exp\left[-\left(\frac{\theta}{E}\right)^b\right] - \frac{\rho}{m} v_{ads} \tag{44}$$

where ρ (g/mL) is the density of the adsorbate, m (g) is the weight of the carbon-based sorbent and v_{ads} (mL) is the volume of the adsorbed phase. According to Equation (41), v_{ads} is considered a constant model parameter.

Brouers–Sotolongo

The Brouers–Sotolongo (BS) model, based on statistical and mathematical considerations, is a recent application of fractal models, being a function equivalent to the deformed exponential, as presented in the nonlinear form below (45) [257,258]:

$$q_e = q_m[1 - \exp(-K_{BS}C_e^\alpha)] \tag{45}$$

where K_{BS} is the model constant (L/mg) and the exponent α (-) is a measure of the width of the sorption energy distribution [186].

5.4.3. CBZ Kinetic and Isotherm Models

Regarding the kinetic models outlined in Table 6, it is possible to verify that the pseudo-second-order model is widely applied in CBZ removal studies. For instance, Jun et al. (2019), who studied different kinetic models (i.e., PFO, PSO, Elovich and intraparticle diffusion), concluded that the PSO model is the model that better fitted the experimental data, based on the values of the correlation coefficients (R^2) [210]. Likewise, Naghdi et al. (2017) adjusted experimental data to different models in their linear and nonlinear form and concluded that PSO fitted better than the linear PSO model. Even if nonlinear PSO R^2 was slightly minor than linear PSO form ($R^{2:}$ 0.946 for nonlinear form and R^2: 0.999 for linear form), the calculated q_e in nonlinear form was similar to experimental q_e [213]. According to Wang and Guo (2020), PSO adjusted better when C is low, i.e., at the final step of the adsorption process and when the adsorbent material has many activated sites [259]. Delgado et al. (2019) suggested that data of CBZ adsorption onto PAC fitted very well onto PFO kinetic model because the R^2_{PFO} was very close to 1 and there was no significant difference between estimated and experimental q_e [159].

Additionally, to PSO and PFO, 2-CFOSM was also suggested as a kinetic model for the CBZ removal: Chen et al. (2017) proposed 2-CFOSM as a kinetic model for the CBZ removal using as adsorbent biochar produced at different temperatures and chemically modified.

This model describes the adsorption kinetics of CBZ on biochar to reveal the effects of varying the carbon structure and mineral composition of biochar on fast and slow adsorption [212].

According to the articles reviewed in this section, the pseudo-second-order may be considered as the most appropriate one to describe the CBZ adsorption onto activated carbon or biochar.

Regarding the isotherm models, Table 6 shows that the models more widely used in CBZ adsorption were Freundlich, Langmuir, Sips, Dubin–Ashtakhov, Redlich–Peterson and modified Brouers–Sotolongo.

Yu et al. (2008) tested the adsorption of CBZ (C_0 = 1 µg/L) onto PICA-activated carbon and F400-activated carbon and fitted the equilibrium data using the Freundlich, Langmuir and Sips nonlinear models, concluding that the Freundlich model fitted better than the other models [45]. In another study from the same research group conducted at the same C_0, it was found that Sips model was superior to the others [209]. This different behavior may be explained by pH differences. While in Yu et al. (2008) the pH of the CBZ solution was not modified, in Yu et al. (2005) the pH was neutral [45,209].

Furthermore, the Freundlich and Langmuir models are special cases of the Sips model while the Sips model is more general [209].

Naghdi et al. (2017) found that CBZ adsorption equilibrium data fitted better the Freundlich model than the Langmuir and partition models. Furthermore, the n-value in Freundlich model was greater than 1, which means that the adsorption was favorable with little heterogeneity [213].

Moreover, Shin et al. (2020) found that Freundlich model fitted better than Langmuir model when CBZ adsorption was carried out onto pristine SCG biochars while the Langmuir isotherm model provided a better agreement than Freundlich model on alkali-modified SCG pristine. This difference may be explained because CBZ reacted with the heterogeneous surface in pristine SCG biochars, while only with a homogeneous surface in alkali-modified SCG pristine [215].

On the other hand, Torrellas Álvarez et al. (2015) showed that the Sips model described better the CBZ adsorption than the usual models, such as Langmuir or Freundlich, since these commonly used adsorption models do not consider the competitive effect occurring in the adsorption process [182].

Similarly, Álvarez-Torrellas et al. (2017) found that Sips and Gab models described better CBZ adsorption than Langmuir or Freundlich since they are highly suitable models to fit multilayer adsorption profiles [211]. To et al. (2017) suggested that the CBZ adsorption on the adsorbents tested may carry out in monolayers because Langmuir isotherm model fitted well [201]. However, the Sips isotherm and the Redlich–Peterson isotherm, which expressed homogeneous or heterogeneous adsorption, also fitted well, which suggests that the adsorption was homogeneous or heterogeneous. This may be explained because of the chemisorption reactions indicated by the best fit kinetic on Ritchie-second order model and the Elovich kinetic model [201].

6. Conclusions

In the first part of this work, the presence of CBZ in the influent and effluent of the wastewater and drinking water treatment plants was discussed. The studies reviewed showed that in wastewater treatment plants CBZ removal is lower than 50% when only secondary treatments are applied and it is better improved when primary or tertiary treatments are also implemented. Moreover, often CBZ removal is negative because of recombination of conjugated compounds within the plant or due to the release by solids. On the other hand, it was seen that in drinking water treatment plants, the treatment which accomplishes major CBZ removal is the adsorption onto Granular Activated Carbon (GAC) and Biological Activated Carbon (BAC) and ozonation. Among adsorbents, activated carbon is usually employed in DWTPs. However, looking at improving the circularity of the water treatment chain, biochar was considered in this review along with activated carbon.

Regarding the adsorbency characteristics, it can be concluded that precursors, pyrolysis temperature and modification or activation processes influence the physico-chemical characteristics of the activated carbon or biochar, and as a consequence CBZ adsorption capacity. The key factors in CBZ removal are S_{BET}, V_{mi} and the presence of aromatic carbon components. Most of the studies analyzed highlighted that an increase of S_{BET} increased CBZ adsorption onto carbonous material. It was seen that an increase of the pyrolysis temperature provokes a higher S_{BET} of carbonous material. Moreover, carbonous material with high V_{mi} presented greater CBZ adsorption capacity, due to CBZ removal by pore-filling mechanisms. In some cases, acid-alkali activation or washing enhance V_{mi}.

Furthermore, carbonous material with a greater aromatic carbon component shows an enhancement of the adsorption capacity so that the adsorption occurs through π-π bond interaction. Among operational conditions of the adsorption process, pH cannot be considered as a very important factor to control because CBZ does not present charge in mostly pH range. In contrast, increasing temperature and rotational speed favors the adsorption of CBZ. The presence of other microcontaminants and organic matter decreases the CBZ adsorption because of competition effects.

Regarding the kinetic models, even among different experimental conditions, a better agreement with the experimental data is obtained more frequently by the PSO, suggesting the chemisorption nature of the adsorption process. However, the main identified mechanism that explains CBZ adsorption is the pore-filling which is characteristic of the adsorption of small-size organic compounds such as CBZ. Other mechanisms which may contribute are hydrophobic and π-π interactions. The isotherms models which best de-

scribed the adsorption process of CBZ at equilibrium, among the studies published, are Freundlich, Langmuir and Sips.

Finally, looking at the stability and reusability of biochar, Inyang and Dickenson (2015) conclude that biochar with a high content of carbon presents stability in soil application, while for water treatment, this property has not been studied [260]. Moreover, Oliveira et al. (2017) showed that the increase in aromaticity and carbon content together enhance the potential stability of biochar [261]. Regarding the reusability of biochar on a large scale, some studies suggested that saturated biochar can be replaced with new or recycled biochar [148].

Overall, quite comprehensive knowledge of the adsorption processes of CBZ in activated carbon and biochar resulted from the reviewed studies. However, these results concern mainly laboratory-scale studies.

7. Future Perspectives

For the future practical engineering application of activated biochar, we should gain insight into the problems regarding its large-scale production, scaled-up application, stability, reuses and the management of spent biochar. Therefore, it is important to continue to study efficient ways to apply and recycle biochar [262]. Furthermore, more studies on its activation and modification are necessary to enhance its adsorption capacity and enable biochar reuse over multiple sorting cycles without suffering stability loss [260]. Moreover, it would be interesting to foresee, according to the described adsorption processes, the treatment conditions suitable for the achievement of removal efficiencies defined based on water quality standards. These quality standards, not currently regulated regarding CBZ, could be identified through risk assessment procedures in case of human consumption and considering different fates of the treated wastewater.

Author Contributions: Conceptualization, data curation, formal analysis, investigation, methodology, writing—original draft, resources, visualization: M.A.D., S.M., C.D.M. and M.B.; supervision, validation, writing—review and editing: A.C. and M.R.B. All authors have read and agreed to the published version of the manuscript.

Institutional Review Board Statement: Not applicable.

Informed Consent Statement: Not applicable.

Data Availability Statement: The data presented in this study is available on request from the corresponding author.

Conflicts of Interest: The authors declare no conflict of interest.

Abbreviations

Abbreviation	Meaning
a_{RP}	Redlich–Peterson constant $[(mg/L)\text{-}n_{RP}]$
AC	Activated carbon
b	Surface heterogeneity (-)
BC	Biochar
BET	Brunauer–Emmett–Teller
BS	Brouers–Sotolongo
C	BET isotherm constant
C_0	Initial concentration (μg/L or mg/L)
C_e	Equilibrium concentration (μg/L or mg/L)
C_s	Adsorbate solubility (mg/L)
CAS	Chemical abstracts service

CBZ	Carbamazepine
CECs	Contaminants of emerging concern
COD	Chemical oxygen demand (mg/L)
d	Average pore width (Å)
D	Average particle size (μm)
DA	Dubinin–Ashtakhov
DO	Dissolved oxygen (mg/L)
DOC	Dissolved organic carbon (mg/L)
DOM	Dissolved organic matter (mg/L)
DWTPs	Drinking water treatment plants
E	Adsorption energy (kJ)
f_f	fraction of the fast compartment (-)
f_s	fraction of the slow compartment (-)
Fd	Frequency of detection (%)
GAB	Guggenheim-Anderson-De Boer
GAC	Granular activated carbon
GW	Groundwater
HRT	Hydraulic retention time
$IN°$	Iodine number (mg/g)
k_1	Rate constant of pseudo-first-order (L/min)
k_2	Rate constant of pseudo-second-order [g/(mg min)]
k_{DC}	Diffusion-chemisorption constant [mg/(g h$^{0.5}$)]
k_f	Rate constant of the fast compartment (1/h)
k_{mr}	Modified Ritchie-second-order rate constant (L/min)
k_r	Ritchie-second-order rate constant (L/min)
k_s	Rate constant of the slow compartment (1/h)
K_1	Equilibrium constants for the first layer (L/mg) in GAB model
K_2	Equilibrium constants for the second layer (L/mg) in GAB model
K_{BS}	Brouers–Sotolongo constant (L/mg)
K_F	Freundlich constant [(mg/mg)(L/mg)$^{1/n}$]
K_H	Henry's law constant (atm·m^3/mol)
K_{HE}	Henry's linear constant (L/g)
K_L	Langmuir constant (L/ng)
K_{ow}	octanol-water partition coefficient (-)
K_{RP}	Redlich–Peterson constant (L/g)
K_S	Sips constant (L/g)
LOD	Limit of detection
LOQ	Limit of quantification
m	Weight of the carbon-based sorbent (g)
MDA	Modified Dubinin–Ashtakov
n	Freundlich nonlinear coefficient (-)
n_{RP}	Redlich–Peterson constant (-)
n_S	Sips constant (-)
PAC	Powdered activated carbon
pH_{IEP}	Isoelectric point (-)
pH_{PZC}	Point of zero charge (-)
pKa	Log of acid dissociation constant
PNEC	Predicted not effects concentration
PFO	Pseudo-first-order
PSO	Pseudo-second-order
q_e	Equilibrium adsorption capacity (mg/g)
$q_{e\ calc}$	Calculated equilibrium adsorption capacity (mg/g)
$q_{e\ exp}$	Experimental equilibrium adsorption capacity (mg/g)
q_m	Maximum adsorption capacity (mg/g)
$q_{m,1}$	Maximum adsorption capacity on the first layer (mg/g)
P/P_0	Relative pressure (-)
R	Removal efficiency (%)

R_{GAS}	Universal gas constant
RW	Raw water
RWW	Raw wastewater
S	Water solubility (mol/L or mg/L)
S_{BET}	Specific surface area (m^2/g)
SR	Speed rotation (rpm)
SW	Surface water
t	Contact time (h)
t_e	Equilibrium time (h)
T	Temperature (°C or °K)
TW	Treated water
v_{ads}	Volume of the adsorbed phase (mL)
V_{me}	Mesopore volumes (cm^3/g)
V_{mi}	Micropore volumes (cm^3/g)
V_T	Total pore volume (cm^3/g)
WTPs	Water treatment plants
WWTPs	Wastewater treatment plants
α	Width of the sorption energy distribution (-)
β_2	Surface coverage of the adsorbent (-)
λ_{ap}	Apparent density (g/mL)
$\Lambda_{particle}$	Particle density (g/mL)
ρ	Contaminant density (g/mL)
θ	Adsorption potential (kJ mol^{-1})

References

1. European Parliament. *Strategic Approach to Pharmaceuticals in the Environment (P9_TA(2020)0226)*; European Parliament: Brussels, Belgium, 2020.
2. Organisation for Economic Co-operation and Development (OECD). *Pharmaceutical Residues in Freshwater Hazards and Policy Responses*; Organisation for Economic Co-operation and Development (OECD): Paris, France, 2019.
3. Di Marcantonio, C.; Chiavola, A.; Dossi, S.; Cecchini, G.; Leoni, S.; Frugis, A.; Spizzirri, M.; Boni, M.R. Occurrence, seasonal variations and removal of Organic Micropollutants in 76 Wastewater Treatment Plants. *Process. Saf. Environ. Prot.* **2020**, *141*, 61–72. [CrossRef]
4. Hai, F.; Yang, S.; Asif, M.; Sencadas, V.; Shawkat, S.; Sanderson-Smith, M.; Gorman, J.; Xu, Z.-Q.; Yamamoto, K. Carbamazepine as a Possible Anthropogenic Marker in Water: Occurrences, Toxicological Effects, Regulations and Removal by Wastewater Treatment Technologies. *Water* **2018**, *10*, 107. [CrossRef]
5. Martínez-Alcalá, I.; Guillén-Navarro, J.M.; Fernández-López, C. Pharmaceutical biological degradation, sorption and mass balance determination in a conventional activated-sludge wastewater treatment plant from Murcia, Spain. *Chem. Eng. J.* **2017**, *316*, 332–340. [CrossRef]
6. Min, X.; Li, W.; Wei, Z.; Spinney, R.; Dionysiou, D.D.; Seo, Y.; Tang, C.J.; Li, Q.; Xiao, R. Sorption and biodegradation of pharmaceuticals in aerobic activated sludge system: A combined experimental and theoretical mechanistic study. *Chem. Eng. J.* **2018**, *342*, 211–219. [CrossRef]
7. Tran, N.H.; Gin, K.Y.H. Occurrence and removal of pharmaceuticals, hormones, personal care products, and endocrine disrupters in a full-scale water reclamation plant. *Sci. Total Environ.* **2017**, *599–600*, 1503–1516. [CrossRef] [PubMed]
8. Santos, L.H.M.L.M.; Araújo, A.N.; Fachini, A.; Pena, A.; Delerue-Matos, C.; Montenegro, M.C.B.S.M. Ecotoxicological aspects related to the presence of pharmaceuticals in the aquatic environment. *J. Hazard. Mater.* **2010**, *175*, 45–95. [CrossRef] [PubMed]
9. Dullio, V.; von der Ohe, P.C. *NORMAN Prioritisation Framework for Emerging Substances*; NORMAN Association: Verneuil-en-Halatte, France, 2013.
10. Webb, S.; Ternes, T.; Gibert, M.; Olejniczak, K. Indirect human exposure to pharmaceuticals via drinking water. *Toxicol. Lett.* **2003**, *142*, 157–167. [CrossRef]
11. Chen, X.; Hu, Z.; Zhang, Y.; Zhuang, L.; Zhang, J.; Li, J.; Hu, H. Removal processes of carbamazepine in constructed wetlands treating secondary effluent: A review. *Water* **2018**, *10*, 1351. [CrossRef]
12. Yao, M.; Duan, L.; Wei, J.; Qian, F.; Hermanowicz, S.W. Carbamazepine removal from wastewater and the degradation mechanism in a submerged forward osmotic membrane bioreactor. *Bioresour. Technol.* **2020**, *314*, 123732. [CrossRef]
13. Amalraj Appavoo, I.; Hu, J.; Huang, Y.; Li, S.F.Y.; Ong, S.L. Response surface modeling of Carbamazepine (CBZ) removal by Graphene-P25 nanocomposites/UVA process using central composite design. *Water Res.* **2014**, *57*, 270–279. [CrossRef]
14. Gurung, K.; Ncibi, M.C.; Shestakova, M.; Sillanpää, M. Removal of carbamazepine from MBR effluent by electrochemical oxidation (EO) using a Ti/Ta2O5-SnO2 electrode. *Appl. Catal. B Environ.* **2018**, *221*, 329–338. [CrossRef]

15. García-Espinoza, J.D.; Nacheva, P.M. Degradation of pharmaceutical compounds in water by oxygenated electrochemical oxidation: Parametric optimization, kinetic studies and toxicity assessment. *Sci. Total Environ.* **2019**, *691*, 417–429. [CrossRef] [PubMed]

16. Yang, B.; Kookana, R.S.; Williams, M.; Du, J.; Doan, H.; Kumar, A. Removal of carbamazepine in aqueous solutions through solar photolysis of free available chlorine. *Water Res.* **2016**, *100*, 413–420. [CrossRef]

17. Baalbaki, A.; Ayoub, G.M.; Al-Hindi, M.; Ghauch, A. The fate of selected pharmaceuticals in solar stills: Transfer, thermal degradation or photolysis? *Sci. Total Environ.* **2017**, *574*, 583–593. [CrossRef]

18. Laera, G.; Chong, M.N.; Jin, B.; Lopez, A. An integrated MBR-TiO2 photocatalysis process for the removal of Carbamazepine from simulated pharmaceutical industrial effluent. *Bioresour. Technol.* **2011**, *102*, 7012–7015. [CrossRef]

19. Gurung, K.; Ncibi, M.C.; Thangaraj, S.K.; Jänis, J.; Seyedsalehi, M.; Sillanpää, M. Removal of pharmaceutically active compounds (PhACs) from real membrane bioreactor (MBR) effluents by photocatalytic degradation using composite Ag2O/P-25 photocatalyst. *Sep. Purif. Technol.* **2019**, *215*, 317–328. [CrossRef]

20. Shahzad, A.; Rasool, K.; Nawaz, M.; Miran, W.; Jang, J.; Moztahida, M.; Mahmoud, K.A.; Lee, D.S. Heterostructural TiO_2/Ti_3C_2Tx (MXene) for photocatalytic degradation of antiepileptic drug carbamazepine. *Chem. Eng. J.* **2018**, *349*, 748–755. [CrossRef]

21. Mahlangu, T.O.; Hoek, E.M.V.; Mamba, B.B.; Verliefde, A.R.D. Influence of organic, colloidal and combined fouling on NF rejection of NaCl and carbamazepine: Role of solute-foulant-membrane interactions and cake-enhanced concentration polarisation. *J. Memb. Sci.* **2014**, *471*, 35–46. [CrossRef]

22. Tang, Y.; Chen, Z.; Wen, Q.; Yang, B.; Pan, Y. Evaluation of a hybrid process of magnetic ion-exchange resin treatment followed by ozonation in secondary effluent organic matter removal. *Sci. Total Environ.* **2021**, *754*, 142361. [CrossRef]

23. Wang, W.; Li, X.; Yuan, S.; Sun, J.; Zheng, S. Effect of resin charged functional group, porosity, and chemical matrix on the long-term pharmaceutical removal mechanism by conventional ion exchange resins. *Chemosphere* **2016**, *160*, 71–79. [CrossRef] [PubMed]

24. Rao, Y.F.; Qu, L.; Yang, H.; Chu, W. Degradation of carbamazepine by Fe(II)-activated persulfate process. *J. Hazard. Mater.* **2014**, *268*, 23–32. [CrossRef] [PubMed]

25. Wang, S.; Zhou, N. Removal of carbamazepine from aqueous solution using sono-activated persulfate process. *Ultrason. Sonochem.* **2016**, *29*, 156–162. [CrossRef]

26. Liu, Y.; Mei, S.; Iya-Sou, D.; Cavadias, S.; Ognier, S. Carbamazepine removal from water by dielectric barrier discharge: Comparison of ex situ and in situ discharge on water. *Chem. Eng. Process. Process. Intensif.* **2012**, *56*, 10–18. [CrossRef]

27. Krause, H.; Schweiger, B.; Prinz, E.; Kim, J.; Steinfeld, U. Degradation of persistent pharmaceuticals in aqueous solutions by a positive dielectric barrier discharge treatment. *J. Electrostat.* **2011**, *69*, 333–338. [CrossRef]

28. Im, J.K.; Cho, I.H.; Kim, S.K.; Zoh, K.D. Optimization of carbamazepine removal in $O_3/UV/H_2O_2$ system using a response surface methodology with central composite design. *Desalination* **2012**, *285*, 306–314. [CrossRef]

29. Liu, N.; Lei, Z.D.; Wang, T.; Wang, J.J.; Zhang, X.D.; Xu, G.; Tang, L. Radiolysis of carbamazepine aqueous solution using electron beam irradiation combining with hydrogen peroxide: Efficiency and mechanism. *Chem. Eng. J.* **2016**, *295*, 484–493. [CrossRef]

30. He, Q.; Liang, J.J.; Chen, L.X.; Chen, S.L.; Zheng, H.L.; Liu, H.X.; Zhang, H.J. Removal of the environmental pollutant carbamazepine using molecular imprinted adsorbents: Molecular simulation, adsorption properties, and mechanisms. *Water Res.* **2020**, *168*, 115164. [CrossRef] [PubMed]

31. Nielsen, L.; Bandosz, T.J. Analysis of the competitive adsorption of pharmaceuticals on waste derived materials. *Chem. Eng. J.* **2016**, *287*, 139–147. [CrossRef]

32. Zhou, Y.; Cheng, G.; Chen, K.; Lu, J.; Lei, J.; Pu, S. Adsorptive removal of bisphenol A, chloroxylenol, and carbamazepine from water using a novel β-cyclodextrin polymer. *Ecotoxicol. Environ. Saf.* **2019**, *170*, 278–285. [CrossRef] [PubMed]

33. Dqbrowski, A. *Adsorption and Its Development and Application for Practical Purposes*, 1st ed.; Elsevier: Amsterdam, The Netherlands, 1999; Volume 120, ISBN 9780080557205.

34. Li, X.; Hai, F.I.; Nghiem, L.D. Simultaneous activated carbon adsorption within a membrane bioreactor for an enhanced micropollutant removal. *Bioresour. Technol.* **2011**, *102*, 5319–5324. [CrossRef]

35. Peralta, M.E.; Mártire, D.O.; Moreno, M.S.; Parolo, M.E.; Carlos, L. Versatile nanoadsorbents based on magnetic mesostructured silica nanoparticles with tailored surface properties for organic pollutants removal. *J. Environ. Chem. Eng.* **2021**, *9*, 104841. [CrossRef]

36. Karimi-Maleh, H.; Ayati, A.; Davoodi, R.; Tanhaei, B.; Karimi, F.; Malekmohammadi, S.; Orooji, Y.; Fu, L.; Sillanpää, M. Recent advances in using of chitosan-based adsorbents for removal of pharmaceutical contaminants: A review. *J. Clean. Prod.* **2021**, *291*, 125880. [CrossRef]

37. Wei, H.; Deng, S.; Huang, Q.; Nie, Y.; Wang, B.; Huang, J.; Yu, G. Regenerable granular carbon nanotubes/alumina hybrid adsorbents for diclofenac sodium and carbamazepine removal from aqueous solution. *Water Res.* **2013**, *47*, 4139–4147. [CrossRef]

38. Martucci, A.; Pasti, L.; Marchetti, N.; Cavazzini, A.; Dondi, F.; Alberti, A. Adsorption of pharmaceuticals from aqueous solutions on synthetic zeolites. *Microporous Mesoporous Mater.* **2012**, *148*, 174–183. [CrossRef]

39. Kim, S.; Gholamirad, F.; Yu, M.; Park, C.M.; Jang, A.; Jang, M.; Taheri-Qazvini, N.; Yoon, Y. Enhanced adsorption performance for selected pharmaceutical compounds by sonicated Ti3C2TX MXene. *Chem. Eng. J.* **2021**, *406*, 126789. [CrossRef]

40. Wurzer, C.; Mašek, O. Feedstock doping using iron rich waste increases the pyrolysis gas yield and adsorption performance of magnetic biochar for emerging contaminants. *Bioresour. Technol.* **2021**, *321*, 124473. [CrossRef] [PubMed]

41. Shin, J.; Kwak, J.; Lee, Y.G.; Kim, S.; Choi, M.; Bae, S.; Lee, S.H.; Park, Y.; Chon, K. Competitive adsorption of pharmaceuticals in lake water and wastewater effluent by pristine and NaOH-activated biochars from spent coffee wastes: Contribution of hydrophobic and π-π interactions. *Environ. Pollut.* **2021**, *270*, 116244. [CrossRef]

42. Mojiri, A.; Baharlooeian, M.; Kazeroon, R.A.; Farraji, H.; Lou, Z. Removal of pharmaceutical micropollutants with integrated biochar and marine microalgae. *Microorganisms* **2021**, *9*, 4. [CrossRef]

43. Lee, Y.-G.; Shin, J.; Kwak, J.; Kim, S.; Son, C.; Cho, K.H.; Chon, K. Effects of NaOH Activation on Adsorptive Removal of Herbicides by Biochars Prepared from Ground Coffee Residues. *Energies* **2021**, *14*, 1297. [CrossRef]

44. Kim, K.A.; Sae, O.O.; Park, P.W.; Park, J.Y. Effect of probenecid on the pharmacokinetics of carbamazepine in healthy subjects. *Eur. J. Clin. Pharmacol.* **2005**, *61*, 275–280. [CrossRef] [PubMed]

45. Yu, Z.; Peldszus, S.; Huck, P.M. Adsorption characteristics of selected pharmaceuticals and an endocrine disrupting compound-Naproxen, carbamazepine and nonylphenol-on activated carbon. *Water Res.* **2008**, *42*, 2873–2882. [CrossRef]

46. National Center for Biotechnology Information PubChem Compound Summary for CID 2554, Carbamazepine. Available online: https://pubchem.ncbi.nlm.nih.gov/compound/Carbamazepine (accessed on 6 April 2021).

47. Williams, A.J.; Grulke, C.M.; Edwards, J.; McEachran, A.D.; Mansouri, K.; Baker, N.C.; Patlewicz, G.; Shah, I.; Wambaugh, J.F.; Judson, R.S.; et al. The CompTox Chemistry Dashboard: A community data resource for environmental chemistry. *J. Cheminform.* **2017**, *9*, 61. [CrossRef] [PubMed]

48. Seeley, I.H. Wastewater Engineering. In *Public Works Engineering*; Macmillan Education: London, UK, 1992; pp. 160–214, ISBN 9780073401188.

49. The European parliament and of the council regulation (EC) No 1907/2006 concerning reach. *Off. J. Eur. Union* **2006**. Available online: https://eur-lex.europa.eu/LexUriServ/LexUriServ.do?uri=OJ:L:2007:136:0003:0280:en:PDF (accessed on 6 April 2021).

50. Loos, R.; Carvalho, R.; António, D.C.; Comero, S.; Locoro, G.; Tavazzi, S.; Paracchini, B.; Ghiani, M.; Lettieri, T.; Blaha, L.; et al. EU-wide monitoring survey on emerging polar organic contaminants in wastewater treatment plant effluents. *Water Res.* **2013**, *47*, 6475–6487. [CrossRef] [PubMed]

51. Thiebault, T.; Boussafir, M.; Le Milbeau, C. Occurrence and removal efficiency of pharmaceuticals in an urban wastewater treatment plant: Mass balance, fate and consumption assessment. *J. Environ. Chem. Eng.* **2017**, *5*, 2894–2902. [CrossRef]

52. Subedi, B.; Kannan, K. Occurrence and fate of select psychoactive pharmaceuticals and antihypertensives in two wastewater treatment plants in New York State, USA. *Sci. Total Environ.* **2015**, *514*, 273–280. [CrossRef] [PubMed]

53. Rivera-Jaimes, J.A.; Postigo, C.; Melgoza-Alemán, R.M.; Aceña, J.; Barceló, D.; López de Alda, M. Study of pharmaceuticals in surface and wastewater from Cuernavaca, Morelos, Mexico: Occurrence and environmental risk assessment. *Sci. Total Environ.* **2018**, *613–614*, 1263–1274. [CrossRef] [PubMed]

54. Wu, M.; Xiang, J.; Que, C.; Chen, F.; Xu, G. Occurrence and fate of psychiatric pharmaceuticals in the urban water system of Shanghai, China. *Chemosphere* **2015**, *138*, 486–493. [CrossRef]

55. Wang, D.; Sui, Q.; Lu, S.G.; Zhao, W.T.; Qiu, Z.F.; Miao, Z.W.; Yu, G. Occurrence and removal of six pharmaceuticals and personal care products in a wastewater treatment plant employing anaerobic/anoxic/aerobic and UV processes in Shanghai, China. *Environ. Sci. Pollut. Res.* **2014**, *21*, 4276–4285. [CrossRef]

56. Yan, Q.; Gao, X.; Huang, L.; Gan, X.M.; Zhang, Y.X.; Chen, Y.P.; Peng, X.Y.; Guo, J.S. Occurrence and fate of pharmaceutically active compounds in the largest municipal wastewater treatment plant in Southwest China: Mass balance analysis and consumption back-calculated model. *Chemosphere* **2014**, *99*, 160–170. [CrossRef]

57. Yu, Y.; Wu, L.; Chang, A.C. Seasonal variation of endocrine disrupting compounds, pharmaceuticals and personal care products in wastewater treatment plants. *Sci. Total Environ.* **2013**, *442*, 310–316. [CrossRef]

58. Lajeunesse, A.; Smyth, S.A.; Barclay, K.; Sauvé, S.; Gagnon, C. Distribution of antidepressant residues in wastewater and biosolids following different treatment processes by municipal wastewater treatment plants in Canada. *Water Res.* **2012**, *46*, 5600–5612. [CrossRef]

59. Martínez-Alcalá, I.; Guillén-Navarro, J.M.; Lahora, A. Occurrence and fate of pharmaceuticals in a wastewater treatment plant from southeast of Spain and risk assessment. *J. Environ. Manag.* **2021**, *279*, 111565. [CrossRef]

60. Čelić, M.; Gros, M.; Farré, M.; Barceló, D.; Petrović, M. Pharmaceuticals as chemical markers of wastewater contamination in the vulnerable area of the Ebro Delta (Spain). *Sci. Total Environ.* **2019**, *652*, 952–963. [CrossRef]

61. Martín, J.; Camacho-Muñoz, D.; Santos, J.L.; Aparicio, I.; Alonso, E. Occurrence of pharmaceutical compounds in wastewater and sludge from wastewater treatment plants: Removal and ecotoxicological impact of wastewater discharges and sludge disposal. *J. Hazard. Mater.* **2012**, *239–240*, 40–47. [CrossRef] [PubMed]

62. Komesli, O.T.; Muz, M.; Ak, M.S.; Bakirdere, S.; Gokcay, C.F. Occurrence, fate and removal of endocrine disrupting compounds (EDCs) in Turkish wastewater treatment plants. *Chem. Eng. J.* **2015**, *277*, 202–208. [CrossRef]

63. Verlicchi, P.; Al Aukidy, M.; Jelic, A.; Petrović, M.; Barceló, D. Comparison of measured and predicted concentrations of selected pharmaceuticals in wastewater and surface water: A case study of a catchment area in the Po Valley (Italy). *Sci. Total Environ.* **2014**, *470–471*, 844–854. [CrossRef] [PubMed]

64. Castiglioni, S.; Zuccato, E.; Fattore, E.; Riva, F.; Terzaghi, E.; Koenig, R.; Principi, P.; Di Guardo, A. Micropollutants in Lake Como water in the context of circular economy: A snapshot of water cycle contamination in a changing pollution scenario. *J. Hazard. Mater.* **2020**, *384*, 121441. [CrossRef]

65. Golovko, O.; Kumar, V.; Fedorova, G.; Randak, T.; Grabic, R. Seasonal changes in antibiotics, antidepressants/psychiatric drugs, antihistamines and lipid regulators in a wastewater treatment plant. *Chemosphere* **2014**, *111*, 418–426. [CrossRef]

66. Gurke, R.; Rößler, M.; Marx, C.; Diamond, S.; Schubert, S.; Oertel, R.; Fauler, J. Occurrence and removal of frequently prescribed pharmaceuticals and corresponding metabolites in wastewater of a sewage treatment plant. *Sci. Total Environ.* **2015**, *532*, 762–770. [CrossRef]

67. Bahlmann, A.; Brack, W.; Schneider, R.J.; Krauss, M. Carbamazepine and its metabolites in wastewater: Analytical pitfalls and occurrence in Germany and Portugal. *Water Res.* **2014**, *57*, 104–114. [CrossRef]

68. Paíga, P.; Santos, L.H.M.L.M.; Ramos, S.; Jorge, S.; Silva, J.G.; Delerue-Matos, C. Presence of pharmaceuticals in the Lis river (Portugal): Sources, fate and seasonal variation. *Sci. Total Environ.* **2016**, *573*, 164–177. [CrossRef] [PubMed]

69. K'oreje, K.O.; Okoth, M.; Van Langenhove, H.; Demeestere, K. Occurrence and treatment of contaminants of emerging concern in the African aquatic environment: Literature review and a look ahead. *J. Environ. Manag.* **2020**, *254*, 109752. [CrossRef] [PubMed]

70. Balakrishna, K.; Rath, A.; Praveenkumarreddy, Y.; Guruge, K.S.; Subedi, B. A review of the occurrence of pharmaceuticals and personal care products in Indian water bodies. *Ecotoxicol. Environ. Saf.* **2017**, *137*, 113–120. [CrossRef]

71. Couto, C.F.; Lange, L.C.; Amaral, M.C.S. Occurrence, fate and removal of pharmaceutically active compounds (PhACs) in water and wastewater treatment plants—A review. *J. Water Process. Eng.* **2019**, *32*, 100927. [CrossRef]

72. Krzeminski, P.; Tomei, M.C.; Karaolia, P.; Langenhoff, A.; Almeida, C.M.R.; Felis, E.; Gritten, F.; Andersen, H.R.; Fernandes, T.; Manaia, C.M.; et al. Performance of secondary wastewater treatment methods for the removal of contaminants of emerging concern implicated in crop uptake and antibiotic resistance spread: A review. *Sci. Total Environ.* **2019**, *648*, 1052–1081. [CrossRef]

73. Jelic, A.; Gros, M.; Ginebreda, A.; Cespedes-Sánchez, R.; Ventura, F.; Petrovic, M.; Barcelo, D. Occurrence, partition and removal of pharmaceuticals in sewage water and sludge during wastewater treatment. *Water Res.* **2011**, *45*, 1165–1176. [CrossRef]

74. Yang, Y.; Ok, Y.S.; Kim, K.H.; Kwon, E.E.; Tsang, Y.F. Occurrences and removal of pharmaceuticals and personal care products (PPCPs) in drinking water and water/sewage treatment plants: A review. *Sci. Total Environ.* **2017**, *596–597*, 303–320. [CrossRef] [PubMed]

75. Zhang, Y.; Geißen, S.U.; Gal, C. Carbamazepine and diclofenac: Removal in wastewater treatment plants and occurrence in water bodies. *Chemosphere* **2008**, *73*, 1151–1161. [CrossRef]

76. Sui, Q.; Cao, X.; Lu, S.; Zhao, W.; Qiu, Z.; Yu, G. Occurrence, sources and fate of pharmaceuticals and personal care products in the groundwater: A review. *Emerg. Contam.* **2015**, *1*, 14–24. [CrossRef]

77. Kleywegt, S.; Pileggi, V.; Yang, P.; Hao, C.; Zhao, X.; Rocks, C.; Thach, S.; Cheung, P.; Whitehead, B. Pharmaceuticals, hormones and bisphenol A in untreated source and finished drinking water in Ontario, Canada—Occurrence and treatment efficiency. *Sci. Total Environ.* **2011**, *409*, 1481–1488. [CrossRef] [PubMed]

78. Pulicharla, R.; Proulx, F.; Behmel, S.; Sérodes, J.B.; Rodriguez, M.J. Occurrence and seasonality of raw and drinking water contaminants of emerging interest in five water facilities. *Sci. Total Environ.* **2021**, *751*, 141748. [CrossRef] [PubMed]

79. Kim, H.; Homan, M. Evaluation of pharmaceuticals and personal care products (PPCPs) in drinking water originating from Lake Erie. *J. Great Lakes Res.* **2020**, *46*, 1321–1330. [CrossRef]

80. Wang, C.; Shi, H.; Adams, C.D.; Gamagedara, S.; Stayton, I.; Timmons, T.; Ma, Y. Investigation of pharmaceuticals in Missouri natural and drinking water using high performance liquid chromatography-tandem mass spectrometry. *Water Res.* **2011**, *45*, 1818–1828. [CrossRef] [PubMed]

81. Glassmeyer, S.T.; Furlong, E.T.; Kolpin, D.W.; Batt, A.L.; Benson, R.; Boone, J.S.; Conerly, O.; Donohue, M.J.; King, D.N.; Kostich, M.S.; et al. Nationwide reconnaissance of contaminants of emerging concern in source and treated drinking waters of the United States. *Sci. Total Environ.* **2017**, *581–582*, 909–922. [CrossRef]

82. Simazaki, D.; Kubota, R.; Suzuki, T.; Akiba, M.; Nishimura, T.; Kunikane, S. Occurrence of selected pharmaceuticals at drinking water purification plants in Japan and implications for human health. *Water Res.* **2015**, *76*, 187–200. [CrossRef]

83. Kim, K.Y.; Ekpe, O.D.; Lee, H.J.; Oh, J.E. Perfluoroalkyl substances and pharmaceuticals removal in full-scale drinking water treatment plants. *J. Hazard. Mater.* **2020**, *400*, 123235. [CrossRef]

84. Nam, S.W.; Jo, B.-I.; Yoon, Y.; Zoh, K.D. Occurrence and removal of selected micropollutants in a water treatment plant. *Chemosphere* **2014**, *95*, 156–165. [CrossRef]

85. Cai, M.Q.; Wang, R.; Feng, L.; Zhang, L.Q. Determination of selected pharmaceuticals in tap water and drinking water treatment plant by high-performance liquid chromatography-triple quadrupole mass spectrometer in Beijing, China. *Environ. Sci. Pollut. Res.* **2015**, *22*, 1854–1867. [CrossRef]

86. Lin, T.; Yu, S.; Chen, W. Occurrence, removal and risk assessment of pharmaceutical and personal care products (PPCPs) in an advanced drinking water treatment plant (ADWTP) around Taihu Lake in China. *Chemosphere* **2016**, *152*, 1–9. [CrossRef]

87. Karki, A.J.; Cappelli, P.; Dirks, C.; Pekar, H.; Hellenäs, K.E.; Rosén, J.; Westerberg, E. New efficient methodology for screening of selected organic micropollutants in raw- and drinking water from 90 Swedish water treatment plants. *Sci. Total Environ.* **2020**, *724*, 138069. [CrossRef]

88. Tröger, R.; Köhler, S.J.; Franke, V.; Bergstedt, O.; Wiberg, K. A case study of organic micropollutants in a major Swedish water source—Removal efficiency in seven drinking water treatment plants and influence of operational age of granulated active carbon filters. *Sci. Total Environ.* **2020**, *706*, 135680. [CrossRef]

89. Azzouz, A.; Ballesteros, E. Influence of seasonal climate differences on the pharmaceutical, hormone and personal care product removal efficiency of a drinking water treatment plant. *Chemosphere* **2013**, *93*, 2046–2054. [CrossRef]

90. Radjenović, J.; Petrović, M.; Ventura, F.; Barceló, D. Rejection of pharmaceuticals in nanofiltration and reverse osmosis membrane drinking water treatment. *Water Res.* **2008**, *42*, 3601–3610. [CrossRef]

91. Valbonesi, P.; Profita, M.; Vasumini, I.; Fabbri, E. Contaminants of emerging concern in drinking water: Quality assessment by combining chemical and biological analysis. *Sci. Total Environ.* **2020**, *758*, 143624. [CrossRef] [PubMed]

92. de Jesus Gaffney, V.; Almeida, C.M.M.; Rodrigues, A.; Ferreira, E.; Benoliel, M.J.; Cardoso, V.V. Occurrence of pharmaceuticals in a water supply system and related human health risk assessment. *Water Res.* **2015**, *72*, 199–208. [CrossRef]

93. Al-Rifai, J.H.; Khabbaz, H.; Schäfer, A.I. Removal of pharmaceuticals and endocrine disrupting compounds in a water recycling process using reverse osmosis systems. *Sep. Purif. Technol.* **2011**, *77*, 60–67. [CrossRef]

94. He, S.; Shi, G.; Xiao, H.; Sun, G.; Shi, Y.; Chen, G.; Dai, H.; Yuan, B.; Chen, X.; Yang, X. Self S-doping activated carbon derived from lignin-based pitch for removal of gaseous benzene. *Chem. Eng. J.* **2021**, *410*, 128286. [CrossRef]

95. Tan, X.-F.; Liu, S.-B.; Liu, Y.-G.; Gu, Y.-L.; Zeng, G.-M.; Hu, X.-J.; Wang, X.; Liu, S.-H.; Jiang, L.-H. Biochar as potential sustainable precursors for activated carbon production: Multiple applications in environmental protection and energy storage. *Bioresour. Technol.* **2017**, *227*, 359–372. [CrossRef]

96. Salomón, Y.L.d.O.; Georgin, J.; Franco, D.S.P.; Netto, M.S.; Piccilli, D.G.A.; Foletto, E.L.; Oliveira, L.F.S.; Dotto, G. High-performance removal of 2,4-dichlorophenoxyacetic acid herbicide in water using activated carbon derived from Queen palm fruit endocarp (Syagrus romanzoffiana). *J. Environ. Chem. Eng.* **2021**, *9*, 104911. [CrossRef]

97. Altıntığ, E.; Yenigun, M.; Sarı, A.; Altundag, H.; Tuzen, M.; Saleh, T.A. Facile synthesis of zinc oxide nanoparticles loaded activated carbon as an eco-friendly adsorbent for ultra-removal of malachite green from water. *Environ. Technol. Innov.* **2021**, *21*, 101305. [CrossRef]

98. Fundneider, T.; Acevedo Alonso, V.; Wick, A.; Albrecht, D.; Lackner, S. Implications of biological activated carbon filters for micropollutant removal in wastewater treatment. *Water Res.* **2021**, *189*, 116588. [CrossRef] [PubMed]

99. Vilardi, G.; Bubbico, R.; Di Palma, L.; Verdone, N. Nitrate green removal by fixed-bed columns packed with waste biomass: Modelling and friction parameter estimation. *Chem. Eng. Res. Des.* **2020**, *154*, 250–261. [CrossRef]

100. Boni, M.R.; Sbaffoni, S.; Tedesco, P.; Vaccari, M. Mass balance of emerging organic micropollutants in a small wastewater treatment plant. *WIT Trans. Ecol. Environ.* **2012**, *164*, 345–356. [CrossRef]

101. Larson, C.D. Historical Development of the National Primary Drinking Water Regulations. In *Safe Drinking Water Act*; CRC Press: Boca Raton, FL, USA, 1989; p. 14, ISBN 9780203710432.

102. Norra, G.F.; Radjenovic, J. Removal of persistent organic contaminants from wastewater using a hybrid electrochemical-granular activated carbon (GAC) system. *J. Hazard. Mater.* **2021**, *415*, 125557. [CrossRef]

103. Rueda-Márquez, J.J.; Moreno-Andrés, J.; Rey, A.; Corada-Fernández, C.; Mikola, A.; Manzano, M.A.; Levchuk, I. Post-treatment of real municipal wastewater effluents by means of granular activated carbon (GAC) based catalytic processes: A focus on abatement of pharmaceutically active compounds. *Water Res.* **2021**, *192*, 116833. [CrossRef] [PubMed]

104. Pagnozzi, G.; Carroll, S.; Reible, D.D.; Millerick, K. Powdered activated carbon (PAC) amendment enhances naphthalene biodegradation under strictly sulfate-reducing conditions. *Environ. Pollut.* **2021**, *268*, 115641. [CrossRef]

105. Alameddine, M.; How, Z.T.; Gamal El-Din, M. Advancing the treatment of primary influent and effluent wastewater during wet weather flow by single versus powdered activated carbon-catalyzed ozonation for the removal of trace organic compounds. *Sci. Total Environ.* **2021**, *770*, 144679. [CrossRef]

106. Qu, J.; Liu, Y.; Cheng, L.; Jiang, Z.; Zhang, G.; Deng, F.; Wang, L.; Han, W.; Zhang, Y. Green synthesis of hydrophilic activated carbon supported sulfide nZVI for enhanced Pb(II) scavenging from water: Characterization, kinetics, isotherms and mechanisms. *J. Hazard. Mater.* **2021**, *403*, 123607. [CrossRef]

107. Jjagwe, J.; Olupot, P.W.; Menya, E.; Kalibbala, H.M. Synthesis and application of Granular activated carbon from biomass waste materials for water treatment: A review. *J. Bioresour. Bioprod.* **2021**, *6*, 292–322. [CrossRef]

108. Juárez-Galán, J.M.; Silvestre-Albero, A.; Silvestre-Albero, J.; Rodríguez-Reinoso, F. Synthesis of activated carbon with highly developed "mesoporosity". *Microporous Mesoporous Mater.* **2009**, *117*, 519–521. [CrossRef]

109. Nakagawa, Y.; Molina-Sabio, M.; Rodríguez-Reinoso, F. Modification of the porous structure along the preparation of activated carbon monoliths with H3PO4 and ZnCl2. *Microporous Mesoporous Mater.* **2007**, *103*, 29–34. [CrossRef]

110. Lamine, S.M.; Ridha, C.; Mahfoud, H.M.; Mouad, C.; Lotfi, B.; Al-Dujaili, A.H. Chemical activation of an activated carbon prepared from coffee residue. In Proceedings of the Energy Procedia; Elsevier Ltd: Amsterdam, The Netherlands, 2014; Volume 50, pp. 393–400.

111. Chi, N.T.L.; Anto, S.; Ahamed, T.S.; Kumar, S.S.; Shanmugam, S.; Samuel, M.S.; Mathimani, T.; Brindhadevi, K.; Pugazhendhi, A. A review on biochar production techniques and biochar based catalyst for biofuel production from algae. *Fuel* **2021**, *287*, 119411. [CrossRef]

112. Boni, M.R.; Chiavola, A.; Antonucci, A.; Di Mattia, E.; Marzeddu, S. A novel treatment for Cd-contaminated solution through adsorption on beech charcoal: The effect of bioactivation. *Desalin. Water Treat.* **2018**, *127*, 104–110. [CrossRef]

113. Novotny, E.H.; Hayes, M.H.B.; Madari, B.E.; Bonagamba, T.J.; de Azevedo, E.R.; de Souza, A.A.; Song, G.; Nogueira, C.M.; Mangrich, A.S. Lessons from the Terra Preta de Índios of the Amazon region for the utilisation of charcoal for soil amendment. *J. Braz. Chem. Soc.* **2009**, *20*, 1003–1010. [CrossRef]

114. Batista, E.M.C.C.; Shultz, J.; Matos, T.T.S.; Fornari, M.R.; Ferreira, T.M.; Szpoganicz, B.; de Freitas, R.A.; Mangrich, A.S. Effect of surface and porosity of biochar on water holding capacity aiming indirectly at preservation of the Amazon biome. *Sci. Rep.* **2018**, *8*, 1–9. [CrossRef]

115. Pandey, S.D.; Mendonça, F.G.; Rodrigues, M.N.; Faria, B.P.Z.; Campos, J.L.E.; Noronha, I.F.P.C.; Vieira, S.S.; Santos, N.A.V.; Fernandes, L.A.; Sampaio, R.A.; et al. Structural and elemental analysis of biochars in the search of a synthetic path to mimetize anthropic Amazon soils. *J. Environ. Manag.* **2021**, *279*, 111685. [CrossRef] [PubMed]

116. Meyer, S.; Glaser, B.; Quicker, P. Technical, Economical, and Climate-Related Aspects of Biochar Production Technologies: A Literature Review. *Environ. Sci. Technol.* **2011**, *45*, 9473–9483. [CrossRef]

117. Akhil, D.; Lakshmi, D.; Kartik, A.; Vo, D.-V.N.; Arun, J.; Gopinath, K.P. Production, characterization, activation and environmental applications of engineered biochar: A review. *Environ. Chem. Lett.* **2021**, *1*, 3. [CrossRef]

118. Chiavola, A.; Marzeddu, S.; Boni, M.R. Remediation of Water Contaminated by Pb(II) Using Virgin Coniferous Wood Biochar as Adsorbent. In *Frontiers in Water-Energy-Nexus—Nature-Based Solutions, Advanced Technologies and Best Practices for Environmental Sustainability. Advances in Science, Technology & Innovation (IEREK Interdisciplinary Series for Sustainable Development)*; Naddeo, V., Balakrishnan, M., Choo, K.-H., Eds.; Springer: Cham, Switzerland; Salerno, Italy, 2020; pp. 363–366, ISBN 978-3-030-13067-1.

119. Gutiérrez, J.; Rubio-Clemente, A.; Pérez, J.F. Effect of main solid biomass commodities of patula pine on biochar properties produced under gasification conditions. *Ind. Crops Prod.* **2021**, *160*, 113123. [CrossRef]

120. Kwoczynski, Z.; Čmelík, J. Characterization of biomass wastes and its possibility of agriculture utilization due to biochar production by torrefaction process. *J. Clean. Prod.* **2021**, *280*, 124302. [CrossRef]

121. Mohamed, B.A.; Ellis, N.; Kim, C.S.; Bi, X.; Chen, W.-H. Engineered biochars from catalytic microwave pyrolysis for reducing heavy metals phytotoxicity and increasing plant growth. *Chemosphere* **2021**, *271*, 129808. [CrossRef] [PubMed]

122. Kumar, M.; Xiong, X.; Wan, Z.; Sun, Y.; Tsang, D.C.W.; Gupta, J.; Gao, B.; Cao, X.; Tang, J.; Ok, Y.S. Ball milling as a mechanochemical technology for fabrication of novel biochar nanomaterials. *Bioresour. Technol.* **2020**, *312*, 123613. [CrossRef] [PubMed]

123. Jeyasubramanian, K.; Thangagiri, B.; Sakthivel, A.; Dhaveethu Raja, J.; Seenivasan, S.; Vallinayagam, P.; Madhavan, D.; Malathi Devi, S.; Rathika, B. A complete review on biochar: Production, property, multifaceted applications, interaction mechanism and computational approach. *Fuel* **2021**, *292*, 120243. [CrossRef]

124. Ding, Y.; Liu, Y.; Liu, S.; Li, Z.; Tan, X.; Huang, X.; Zeng, G.; Zhou, L.; Zheng, B. Biochar to improve soil fertility. A review. *Agron. Sustain. Dev.* **2016**, *36*, 1–18. [CrossRef]

125. Jindo, K.; Audette, Y.; Higashikawa, F.S.; Silva, C.A.; Akashi, K.; Mastrolonardo, G.; Sánchez-Monedero, M.A.; Mondini, C. Role of biochar in promoting circular economy in the agriculture sector. Part 1: A review of the biochar roles in soil N, P and K cycles. *Chem. Biol. Technol. Agric.* **2020**, *7*, 1–12. [CrossRef]

126. Agegnehu, G.; Bass, A.M.; Nelson, P.N.; Bird, M.I. Benefits of biochar, compost and biochar-compost for soil quality, maize yield and greenhouse gas emissions in a tropical agricultural soil. *Sci. Total Environ.* **2016**, *543*, 295–306. [CrossRef]

127. Giagnoni, L.; Maienza, A.; Baronti, S.; Vaccari, F.P.; Genesio, L.; Taiti, C.; Martellini, T.; Scodellini, R.; Cincinelli, A.; Costa, C.; et al. Long-term soil biological fertility, volatile organic compounds and chemical properties in a vineyard soil after biochar amendment. *Geoderma* **2019**, *344*, 127–136. [CrossRef]

128. Gao, Y.; Shao, G.; Lu, J.; Zhang, K.; Wu, S.; Wang, Z. Effects of biochar application on crop water use efficiency depend on experimental conditions: A meta-analysis. *F. Crop. Res.* **2020**, *249*, 107763. [CrossRef]

129. Oldfield, T.L.; Sikirica, N.; Mondini, C.; López, G.; Kuikman, P.J.; Holden, N.M. Biochar, compost and biochar-compost blend as options to recover nutrients and sequester carbon. *J. Environ. Manag.* **2018**, *218*, 465–476. [CrossRef]

130. Alhashimi, H.A.; Aktas, C.B. Life cycle environmental and economic performance of biochar compared with activated carbon: A meta-analysis. *Resour. Conserv. Recycl.* **2017**, *118*, 13–26. [CrossRef]

131. Soo Kim, H.; Rae Kim, K.; Yang, J.-E.; Sik Ok, Y.; Il Kim, W.; Kunhikrishnan, A.; Kim, K.-H. Amelioration of Horticultural Growing Media Properties Through Rice Hull Biochar Incorporation. *Waste Biomass Valorization* **2017**, *8*, 483–492. [CrossRef]

132. Blok, C.; van der Salm, C.; Hofland-Zijlstra, J.; Streminska, M.; Eveleens, B.; Regelink, I.; Fryda, L.; Visser, R. Biochar for Horticultural Rooting Media Improvement: Evaluation of Biochar from Gasification and Slow Pyrolysis. *Agronomy* **2017**, *7*, 6. [CrossRef]

133. Chrysargyris, A.; Prasad, M.; Kavanagh, A.; Tzortzakis, N. Biochar type, ratio, and nutrient levels in growing media affects seedling production and plant performance. *Agronomy* **2020**, *10*, 1421. [CrossRef]

134. Yu, P.; Huang, L.; Li, Q.; Lima, I.M.; White, P.M.; Gu, M. Effects of mixed hardwood and sugarcane biochar as bark-based substrate substitutes on container plants production and nutrient leaching. *Agronomy* **2020**, *10*, 156. [CrossRef]

135. Huang, L.; Gu, M. Effects of Biochar on Container Substrate Properties and Growth of Plants—A Review. *Horticulturae* **2019**, *5*, 14. [CrossRef]

136. Viotti, P.; Tatti, F.; Rossi, A.; Luciano, A.; Marzeddu, S.; Mancini, G.; Boni, M.R. An Eco-Balanced and Integrated Approach for a More-Sustainable MSW Management. *Waste Biomass Valorization* **2020**, *11*, 5139–5150. [CrossRef]

137. Malyan, S.K.; Kumar, S.S.; Fagodiya, R.K.; Ghosh, P.; Kumar, A.; Singh, R.; Singh, L. Biochar for environmental sustainability in the energy-water-agroecosystem nexus. *Renew. Sustain. Energy Rev.* **2021**, *149*, 111379. [CrossRef]

138. Criscuoli, I.; Ventura, M.; Sperotto, A.; Panzacchi, P.; Tonon, G. Effect of woodchips biochar on sensitivity to temperature of soil greenhouse gases emissions. *Forests* **2019**, *10*, 594. [CrossRef]

139. Mandal, S.; Pu, S.; Adhikari, S.; Ma, H.; Kim, D.H.; Bai, Y.; Hou, D. Progress and future prospects in biochar composites: Application and reflection in the soil environment. *Crit. Rev. Environ. Sci. Technol.* **2021**, *51*, 219–271. [CrossRef]

140. Chen, W.; Meng, J.; Han, X.; Lan, Y.; Zhang, W. Past, present, and future of biochar. *Biochar* **2019**, *1*, 75–87. [CrossRef]

141. Bolognesi, S.; Bernardi, G.; Callegari, A.; Dondi, D.; Capodaglio, A.G. Biochar production from sewage sludge and microalgae mixtures: Properties, sustainability and possible role in circular economy. *Biomass Convers. Biorefinery* **2021**, *11*, 289–299. [CrossRef]

142. Hu, Q.; Jung, J.; Chen, D.; Leong, K.; Song, S.; Li, F.; Mohan, B.C.; Yao, Z.; Prabhakar, A.K.; Lin, X.H.; et al. Biochar industry to circular economy. *Sci. Total Environ.* **2021**, *757*, 143820. [CrossRef] [PubMed]

143. Bassano, C.; Deiana, P.; Vilardi, G.; Verdone, N. Modeling and economic evaluation of carbon capture and storage technologies integrated into synthetic natural gas and power-to-gas plants. *Appl. Energy* **2020**, *263*, 114590. [CrossRef]

144. Mohan, D.; Sarswat, A.; Ok, Y.S.; Pittman, C.U. Organic and inorganic contaminants removal from water with biochar, a renewable, low cost and sustainable adsorbent—A critical review. *Bioresour. Technol.* **2014**, *160*, 191–202. [CrossRef]

145. Vithanage, M.; Ashiq, A.; Ramanayaka, S.; Bhatnagar, A. Implications of layered double hydroxides assembled biochar composite in adsorptive removal of contaminants: Current status and future perspectives. *Sci. Total Environ.* **2020**, *737*, 139718. [CrossRef]

146. Singh, A.; Sharma, R.; Pant, D.; Malaviya, P. Engineered algal biochar for contaminant remediation and electrochemical applications. *Sci. Total Environ.* **2021**, *774*, 145676. [CrossRef]

147. Hu, B.; Ai, Y.; Jin, J.; Hayat, T.; Alsaedi, A.; Zhuang, L.; Wang, X. Efficient elimination of organic and inorganic pollutants by biochar and biochar-based materials. *Biochar* **2020**, *2*, 47–64. [CrossRef]

148. Sizmur, T.; Fresno, T.; Akgül, G.; Frost, H.; Moreno-Jiménez, E. Biochar modification to enhance sorption of inorganics from water. *Bioresour. Technol.* **2017**, *246*, 34–47. [CrossRef]

149. Cheng, N.; Wang, B.; Wu, P.; Lee, X.; Xing, Y.; Chen, M.; Gao, B. Adsorption of emerging contaminants from water and wastewater by modified biochar: A review. *Environ. Pollut.* **2021**, *273*, 116448. [CrossRef]

150. Asimakopoulos, G.; Baikousi, M.; Salmas, C.; Bourlinos, A.B.; Zboril, R.; Karakassides, M.A. Advanced Cr(VI) sorption properties of activated carbon produced via pyrolysis of the "Posidonia oceanica" seagrass. *J. Hazard. Mater.* **2021**, *405*, 124274. [CrossRef] [PubMed]

151. Duan, D.; Chen, D.; Huang, L.; Zhang, Y.; Zhang, Y.; Wang, Q.; Xiao, G.; Zhang, W.; Lei, H.; Ruan, R. Activated carbon from lignocellulosic biomass as catalyst: A review of the applications in fast pyrolysis process. *J. Anal. Appl. Pyrolysis* **2021**, *158*, 105246. [CrossRef]

152. Mariana, M.; Abdul Khalil, H.P.S.; Mistar, E.M.; Yahya, E.B.; Alfatah, T.; Danish, M.; Amayreh, M. Recent advances in activated carbon modification techniques for enhanced heavy metal adsorption. *J. Water Process. Eng.* **2021**, *43*, 102221. [CrossRef]

153. Tomczyk, A.; Sokołowska, Z.; Boguta, P. Biochar physicochemical properties: Pyrolysis temperature and feedstock kind effects. Rev. Environ. *Sci. Bio/Technol.* **2020**, *19*, 191–215. [CrossRef]

154. Sajjadi, B.; Chen, W.Y.; Egiebor, N.O. A comprehensive review on physical activation of biochar for energy and environmental applications. *Rev. Chem. Eng.* **2019**, *35*, 735–776. [CrossRef]

155. Jutakridsada, P.; Prajaksud, C.; Kuboonya-Aruk, L.; Theerakulpisut, S.; Kamwilaisak, K. Adsorption characteristics of activated carbon prepared from spent ground coffee. *Clean Technol. Environ. Policy* **2016**, *18*, 639–645. [CrossRef]

156. Demiral, H.; Gündüzoğlu, G. Removal of nitrate from aqueous solutions by activated carbon prepared from sugar beet bagasse. *Bioresour. Technol.* **2010**, *101*, 1675–1680. [CrossRef]

157. Lange, S.F.; Allaire, S.E.; Charles, A.; Auclair, I.K.; Bajzak, C.E.; Turgeon, L.; St-Gelais, A. *Physicochemical Properties of 43 Biochars*; Centre de Recherche sur les Matériaux Renouvelables, Université: Quebec, QC, Canada, 2018.

158. Yakout, S.M.; Sharaf El-Deen, G. Characterization of activated carbon prepared by phosphoric acid activation of olive stones. *Arab. J. Chem.* **2016**, *9*, S1155–S1162. [CrossRef]

159. Delgado, N.; Capparelli, A.; Navarro, A.; Marino, D. Pharmaceutical emerging pollutants removal from water using powdered activated carbon: Study of kinetics and adsorption equilibrium. *J. Environ. Manag.* **2019**, *236*, 301–308. [CrossRef]

160. Khadiran, T.; Hussein, M.Z.; Zainal, Z.; Rusli, R. Textural and chemical properties of activated carbon prepared from tropical peat soil by chemical activation method. *BioResources* **2015**, *10*, 986–1007. [CrossRef]

161. Negara, D.N.K.P.; Nindhia, T.G.T.; Surata, I.W.; Hidajat, F.; Sucipta, M. Textural characteristics of activated carbons derived from tabah bamboo manufactured by using H3PO4 chemical activation. *Mater. Today Proc.* **2020**, *22*, 148–155. [CrossRef]

162. Azargohar, R.; Dalai, A.K. Biochar As a Precursor of Activated Carbon. In *Twenty-Seventh Symposium on Biotechnology for Fuels and Chemicals*; Humana Press: Totowa, NJ, USA, 2007; pp. 762–773. [CrossRef]

163. Yahya, M.A.; Al-Qodah, Z.; Ngah, C.W.Z. Agricultural bio-waste materials as potential sustainable precursors used for activated carbon production: A review. *Renew. Sustain. Energy Rev.* **2015**, *46*, 218–235. [CrossRef]

164. Liu, Z.; Dugan, B.; Masiello, C.A.; Gonnermann, H.M. Biochar particle size, shape, and porosity act together to influence soil water properties. *PLoS ONE* **2017**, *12*, e0179079. [CrossRef]

165. Maulina, S.; Iriansyah, M. Characteristics of activated carbon resulted from pyrolysis of the oil palm fronds powder. *IOP Conf. Ser. Mater. Sci. Eng.* **2018**, *309*, 012072. [CrossRef]

166. Qian, Q.; Machida, M.; Tatsumoto, H. Textural and surface chemical characteristics of activated carbons prepared from cattle manure compost. *Waste Manag.* **2008**, *28*, 1064–1071. [CrossRef]

167. Acevedo, S.; Giraldo, L.; Moreno-Piraján, J.C. Adsorption of CO2 onto Activated Carbons Prepared by Chemical Activation with Metallic Salts. *Int. J. Chem. React. Eng.* **2018**, *15*, 1–12. [CrossRef]

168. Breton, L.A.; Mahdi, Z.; Pratt, C.; Hanandeh, A. El Modification of Hardwood Derived Biochar to Improve Phosphorus Adsorption. *Environmental* **2021**, *8*, 41. [CrossRef]
169. Nielsen, L.; Biggs, M.J.; Skinner, W.; Bandosz, T.J. The effects of activated carbon surface features on the reactive adsorption of carbamazepine and sulfamethoxazole. *Carbon N. Y.* **2014**, *80*, 419–432. [CrossRef]
170. Mukhtar, A.; Mellon, N.; Saqib, S.; Lee, S.-P.; Bustam, M.A. Extension of BET theory to CO2 adsorption isotherms for ultra-microporosity of covalent organic polymers. *SN Appl. Sci.* **2020**, *2*, 1232. [CrossRef]
171. Sinha, P.; Datar, A.; Jeong, C.; Deng, X.; Chung, Y.G.; Lin, L.-C. Surface Area Determination of Porous Materials Using the Brunauer–Emmett–Teller (BET) Method: Limitations and Improvements. *J. Phys. Chem. C* **2019**, *123*, 20195–20209. [CrossRef]
172. Brunauer, S.; Emmett, P.H.; Teller, E. Adsorption of Gases in Multimolecular Layers. *J. Am. Chem. Soc.* **1938**, *60*, 309–319. [CrossRef]
173. Zhao, J.; Xu, H.; Tang, D.; Mathews, J.P.; Li, S.; Tao, S. A comparative evaluation of coal specific surface area by CO_2 and N_2 adsorption and its influence on CH4 adsorption capacity at different pore sizes. *Fuel* **2016**, *183*, 420–431. [CrossRef]
174. Ladavos, A.K.; Katsoulidis, A.P.; Iosifidis, A.; Triantafyllidis, K.S.; Pinnavaia, T.J.; Pomonis, P.J. The BET equation, the inflection points of N2 adsorption isotherms and the estimation of specific surface area of porous solids. *Microporous Mesoporous Mater.* **2012**, *151*, 126–133. [CrossRef]
175. Mianowski, A.; Owczarek, M.; Marecka, A. Surface Area of Activated Carbon Determined by the Iodine Adsorption Number. Energy Sources, Part. A Recover. *Util. Environ. Eff.* **2007**, *29*, 839–850. [CrossRef]
176. Wiener, M.; Reichenauer, G.; Scherb, T.; Fricke, J. Accelerating the synthesis of carbon aerogel precursors. *J. Non. Cryst. Solids* **2004**, *350*, 126–130. [CrossRef]
177. Kemball, C.; Schreiner, G.D.L. The Determination of Heats of Adsorption by the Brunauer—Emmett—Teller Single Isotherm Method. *J. Am. Chem. Soc.* **1950**, *72*, 5605–5607. [CrossRef]
178. Singh, G.; Aher, S.C.; Varma, P.V.S.; Sathe, D.B.; Bhatt, R.B. Analysis of BET specific surface area in several recycled oxide powders. *J. Radioanal. Nucl. Chem.* **2021**, *327*, 555–564. [CrossRef]
179. Scherdel, C.; Reichenauer, G.; Wiener, M. Relationship between pore volumes and surface areas derived from the evaluation of N2-sorption data by DR-, BET- and t-plot. *Microporous Mesoporous Mater.* **2010**, *132*, 572–575. [CrossRef]
180. Buttersack, C.; Möllmer, J.; Hofmann, J.; Gläser, R. Determination of micropore volume and external surface of zeolites. *Microporous Mesoporous Mater.* **2016**, *236*, 63–70. [CrossRef]
181. Al-Degs, Y.S.; El-Barghouthi, M.I.; Khraisheh, M.A.; Ahmad, M.N.; Allen, S.J. Effect of Surface Area, Micropores, Secondary Micropores, and Mesopores Volumes of Activated Carbons on Reactive Dyes Adsorption from Solution. *Sep. Sci. Technol.* **2005**, *39*, 97–111. [CrossRef]
182. Alvarez Torrellas, S.; García Lovera, R.; Escalona, N.; Sepúlveda, C.; Sotelo, J.L.; García, J. Chemical-activated carbons from peach stones for the adsorption of emerging contaminants in aqueous solutions. *Chem. Eng. J.* **2015**, *279*, 788–798. [CrossRef]
183. Tay, T.; Ucar, S.; Karagöz, S. Preparation and characterization of activated carbon from waste biomass. *J. Hazard. Mater.* **2009**, *165*, 481–485. [CrossRef]
184. De Lange, M.F.; Vlugt, T.J.H.; Gascon, J.; Kapteijn, F. Adsorptive characterization of porous solids: Error analysis guides the way. *Microporous Mesoporous Mater.* **2014**, *200*, 199–215. [CrossRef]
185. Kenvin, J.; Jagiello, J.; Mitchell, S.; Pérez-Ramírez, J. Unified method for the total pore volume and pore size distribution of hierarchical zeolites from argon adsorption and mercury intrusion. *Langmuir* **2015**, *31*, 1242–1247. [CrossRef]
186. Ncibi, M.C.; Sillanpää, M. Optimizing the removal of pharmaceutical drugs Carbamazepine and Dorzolamide from aqueous solutions using mesoporous activated carbons and multi-walled carbon nanotubes. *J. Mol. Liq.* **2017**, *238*, 379–388. [CrossRef]
187. Wijitkosum, S.; Jiwnok, P. Elemental Composition of Biochar Obtained from Agricultural Waste for Soil Amendment and Carbon Sequestration. *Appl. Sci.* **2019**, *9*, 3980. [CrossRef]
188. Barrett, E.P.; Joyner, L.G.; Halenda, P.P. The Determination of Pore Volume and Area Distributions in Porous Substances. I. Computations from Nitrogen Isotherms. *J. Am. Chem. Soc.* **1951**, *73*, 373–380. [CrossRef]
189. He, S.; Chen, G.; Xiao, H.; Shi, G.; Ruan, C.; Ma, Y.; Dai, H.; Yuan, B.; Chen, X.; Yang, X. Facile preparation of N-doped activated carbon produced from rice husk for CO_2 capture. *J. Colloid Interface Sci.* **2021**, *582*, 90–101. [CrossRef] [PubMed]
190. Settelein, J.; Oehm, J.; Bozkaya, B.; Leicht, H.; Wiener, M.; Reichenauer, G.; Sextl, G. The external surface area of carbon additives as key to enhance the dynamic charge acceptance of lead-carbon electrodes. *J. Energy Storage* **2018**, *15*, 196–204. [CrossRef]
191. Rodríguez-Ramírez, J.; Méndez-Lagunas, L.; López-Ortiz, A.; Torres, S.S. True Density and Apparent Density During the Drying Process for Vegetables and Fruits: A Review. *J. Food Sci.* **2012**, *77*, R146–R154. [CrossRef] [PubMed]
192. Viana, M. About pycnometric density measurements. *Talanta* **2002**, *57*, 583–593. [CrossRef]
193. Huerta-Pujol, O.; Soliva, M.; Martínez-Farré, F.X.; Valero, J.; López, M. Bulk density determination as a simple and complementary tool in composting process control. *Bioresour. Technol.* **2010**, *101*, 995–1001. [CrossRef] [PubMed]
194. Basso, A.S.; Miguez, F.E.; Laird, D.A.; Horton, R.; Westgate, M. Assessing potential of biochar for increasing water-holding capacity of sandy soils. *GCB Bioenergy* **2013**, *5*, 132–143. [CrossRef]
195. Du, C.; Liu, B.; Hu, J.; Li, H. Determination of iodine number of activated carbon by the method of ultraviolet–visible spectroscopy. *Mater. Lett.* **2021**, *285*, 129137. [CrossRef]
196. Mopoung, S.; Moonsri, P.; Palas, W.; Khumpai, S. Characterization and Properties of Activated Carbon Prepared from Tamarind Seeds by KOH Activation for Fe(III) Adsorption from Aqueous Solution. *Sci. World J.* **2015**, *2015*, 1–9. [CrossRef] [PubMed]

197. Babatunde, O.A.; Garba, S.; Ali, Z.N. Surface modification of activated carbon for improved iodine and carbon tetrachloride adsorption. *Am. J. Chem.* **2016**, *6*, 74–79. [CrossRef]

198. Anisuzzaman, S.M.; Joseph, C.G.; Daud, W.M.A.B.W.; Krishnaiah, D.; Yee, H.S. Preparation and characterization of activated carbon from Typha orientalis leaves. *Int. J. Ind. Chem.* **2015**, *6*, 9–21. [CrossRef]

199. Menéndez, J.A.; Illán-Gómez, M.J.; y León, C.A.L.; Radovic, L.R. On the difference between the isoelectric point and the point of zero charge of carbons. *Carbon N. Y.* **1995**, *33*, 1655–1657. [CrossRef]

200. Fiol, N.; Villaescusa, I. Determination of sorbent point zero charge: Usefulness in sorption studies. *Environ. Chem. Lett.* **2009**, *7*, 79–84. [CrossRef]

201. To, M.H.; Hadi, P.; Hui, C.W.; Lin, C.S.K.; McKay, G. Mechanistic study of atenolol, acebutolol and carbamazepine adsorption on waste biomass derived activated carbon. *J. Mol. Liq.* **2017**, *241*, 386–398. [CrossRef]

202. El-Sayed, G.O.; Yehia, M.M.; Asaad, A.A. Assessment of activated carbon prepared from corncob by chemical activation with phosphoric acid. *Water Resour. Ind.* **2014**, *7–8*, 66–75. [CrossRef]

203. Ekpete, O.A.; Marcus, A.C.; Osi, V. Preparation and Characterization of Activated Carbon Obtained from Plantain (Musa paradisiaca) Fruit Stem. *J. Chem.* **2017**, *2017*, 1–6. [CrossRef]

204. Zhang, K.; Mao, J.; Chen, B. Reconsideration of heterostructures of biochars: Morphology, particle size, elemental composition, reactivity and toxicity. *Environ. Pollut.* **2019**, *254*, 113017. [CrossRef] [PubMed]

205. Wang, T.; Camps-Arbestain, M.; Hedley, M. Predicting C aromaticity of biochars based on their elemental composition. *Org. Geochem.* **2013**, *62*, 1–6. [CrossRef]

206. Guo, Y.; Tan, C.; Sun, J.; Li, W.; Zhang, J.; Zhao, C. Porous activated carbons derived from waste sugarcane bagasse for CO2 adsorption. *Chem. Eng. J.* **2020**, *381*, 122736. [CrossRef]

207. Belhachemi, M.; Jeguirim, M.; Limousy, L.; Addoun, F. Comparison of NO2 removal using date pits activated carbon and modified commercialized activated carbon via different preparation methods: Effect of porosity and surface chemistry. *Chem. Eng. J.* **2014**, *253*, 121–129. [CrossRef]

208. Liu, J.; Wu, L.; Chen, X. Kinetic model investigation on lead(II) adsorption using silica-based hybrid membranes. *Desalin. Water Treat.* **2015**, *54*, 2307–2313. [CrossRef]

209. Yu, Z.; Huck, P.M.; Peldszus, S.; Anderson, W.B. Adsorption of selected pharmaceuticals and endocrine disrupting substances by GAC at low concentration levels. In Proceedings of the Water Quality Technology Conference Proceedings, WQTC 2005, Quebec City, QC, Canada, 6–10 November 2005; pp. 1–16.

210. Jun, B.M.; Heo, J.; Park, C.M.; Yoon, Y. Comprehensive evaluation of the removal mechanism of carbamazepine and ibuprofen by metal organic framework. *Chemosphere* **2019**, *235*, 527–537. [CrossRef]

211. Álvarez-Torrellas, S.; Peres, J.A.; Gil-Álvarez, V.; Ovejero, G.; García, J. Effective adsorption of non-biodegradable pharmaceuticals from hospital wastewater with different carbon materials. *Chem. Eng. J.* **2017**, *320*, 319–329. [CrossRef]

212. Chen, J.; Zhang, D.; Zhang, H.; Ghosh, S.; Pan, B. Fast and slow adsorption of carbamazepine on biochar as affected by carbon structure and mineral composition. *Sci. Total Environ.* **2017**, *579*, 598–605. [CrossRef]

213. Naghdi, M.; Taheran, M.; Pulicharla, R.; Rouissi, T.; Brar, S.K.; Verma, M.; Surampalli, R.Y. Pine-wood derived nanobiochar for removal of carbamazepine from aqueous media: Adsorption behavior and influential parameters. *Arab. J. Chem.* **2017**, *12*, 5292–5301. [CrossRef]

214. Dickenson, E.R.V.; Drewes, J.E. Quantitative structure property relationships for the adsorption of pharmaceuticals onto activated carbon. *Water Sci. Technol.* **2010**, *62*, 2270–2276. [CrossRef] [PubMed]

215. Shin, J.; Lee, Y.G.; Lee, S.H.; Kim, S.; Ochir, D.; Park, Y.; Kim, J.; Chon, K. Single and competitive adsorptions of micropollutants using pristine and alkali-modified biochars from spent coffee grounds. *J. Hazard. Mater.* **2020**, *400*, 123102. [CrossRef] [PubMed]

216. Fernández-Reyes, B.; Morales-Jiménez, S.; Muñoz-Senmache, J.C.; Vega-Santander, D.R.; Hernández-Maldonado, A.J. Single- and multi-component adsorption of selected contaminants of emerging concern from water and some of their metabolites onto hierarchical porous copper(II)-zeolite -activated carbon composite. *Microporous Mesoporous Mater.* **2021**, *312*, 110355. [CrossRef]

217. Turk Sekulic, M.; Boskovic, N.; Slavkovic, A.; Garunovic, J.; Kolakovic, S.; Pap, S. Surface functionalised adsorbent for emerging pharmaceutical removal: Adsorption performance and mechanisms. *Process. Saf. Environ. Prot.* **2019**, *125*, 50–63. [CrossRef]

218. Chu, G.; Zhao, J.; Liu, Y.; Lang, D.; Wu, M.; Pan, B.; Steinberg, C.E.W. The relative importance of different carbon structures in biochars to carbamazepine and bisphenol A sorption. *J. Hazard. Mater.* **2019**, *373*, 106–114. [CrossRef]

219. El Mouchtari, E.M.; Daou, C.; Rafqah, S.; Najjar, F.; Anane, H.; Piram, A.; Hamade, A.; Briche, S.; Wong-Wah-Chung, P. TiO$_2$ and activated carbon of Argania Spinosa tree nutshells composites for the adsorption photocatalysis removal of pharmaceuticals from aqueous solution. *J. Photochem. Photobiol. A Chem.* **2020**, *388*, 112183. [CrossRef]

220. Suriyanon, N.; Punyapalakul, P.; Ngamcharussrivichai, C. Mechanistic study of diclofenac and carbamazepine adsorption on functionalized silica-based porous materials. *Chem. Eng. J.* **2013**, *214*, 208–218. [CrossRef]

221. Quesada, H.B.; Baptista, A.T.A.; Cusioli, L.F.; Seibert, D.; de Oliveira Bezerra, C.; Bergamasco, R. Surface water pollution by pharmaceuticals and an alternative of removal by low-cost adsorbents: A review. *Chemosphere* **2019**, *222*, 766–780. [CrossRef]

222. Shan, D.; Deng, S.; Zhao, T.; Wang, B.; Wang, Y.; Huang, J.; Yu, G.; Winglee, J.; Wiesner, M.R. Preparation of ultrafine magnetic biochar and activated carbon for pharmaceutical adsorption and subsequent degradation by ball milling. *J. Hazard. Mater.* **2016**, *305*, 156–163. [CrossRef] [PubMed]

223. Walker, G.M.; Hansen, L.; Hanna, J.A.; Allen, S.J. Kinetics of a reactive dye adsorption onto dolomitic sorbents. *Water Res.* **2003**, *37*, 2081–2089. [CrossRef]

224. Rosales, E.; Meijide, J.; Pazos, M.; Sanromán, M.A. Challenges and recent advances in biochar as low-cost biosorbent: From batch assays to continuous-flow systems. *Bioresour. Technol.* **2017**, *246*, 176–192. [CrossRef] [PubMed]

225. Largitte, L.; Pasquier, R. A review of the kinetics adsorption models and their application to the adsorption of lead by an activated carbon. *Chem. Eng. Res. Des.* **2016**, *109*, 495–504. [CrossRef]

226. Sophia, A.C.; Lima, E.C.; Carmalin, S.A.; Lima, E.C. Removal of emerging contaminants from the environment by adsorption. *Ecotoxicol. Environ. Saf.* **2018**, *150*, 1–17. [CrossRef] [PubMed]

227. Lagergren, S.Y. Zur theorie der sogenannten adsorption geloster stoffe, Kungliga Svenska Vetenskapsakademiens. *Handlingar* **1898**, *24*, 1–39.

228. Boni, M.R; Chiavola, A.; Di Marcantonio, C.; Sbaffoni, S.; Biagioli, S.; Cecchini, G.; Frugis, A. A study through batch tests on the analytical determination and the fate and removal of methamphetamine in the biological treatment of domestic wastewater. *Environ. Sci. Pollut. Res.* **2018**, *25*, 27756–27767. [CrossRef]

229. Ho, Y.S.; McKay, G. Pseudo-second order model for sorption processes. *Process. Biochem.* **1999**, *34*, 451–465. [CrossRef]

230. Ali, R.M.; Hamad, H.A.; Hussein, M.M.; Malash, G.F. Potential of using green adsorbent of heavy metal removal from aqueous solutions: Adsorption kinetics, isotherm, thermodynamic, mechanism and economic analysis. *Ecol. Eng.* **2016**, *91*, 317–332. [CrossRef]

231. Ho, Y.S.; Porter, J.F.; McKay, G. Equilibrium isotherm studies for the sorption of divalent metal ions onto peat: Copper, nickel and lead single component systems. *Water Air Soil Pollut.* **2002**, *141*, 1–33. [CrossRef]

232. Boni, M.R.; Chiavola, A.; Marzeddu, S. Remediation of Lead-Contaminated Water by Virgin Coniferous Wood Biochar Adsorbent: Batch and Column Application. *Water Air Soil Pollut.* **2020**, *231*, 171. [CrossRef]

233. Boni, M.R.; Chiavola, A.; Marzeddu, S. Application of Biochar to the Remediation of Pb-Contaminated Solutions. *Sustainability* **2018**, *10*, 4440. [CrossRef]

234. Ritchie, A.G. Alternative to the Elovich equation for the kinetics of adsorption of gases on solids. *J. Chem. Soc. Faraday Trans. 1 Phys. Chem. Condens. Phases* **1977**, *73*, 1650–1653. [CrossRef]

235. Ho, Y.S. Second-order kinetic model for the sorption of cadmium onto tree fern: A comparison of linear and non-linear methods. *Water Res.* **2006**, *40*, 119–125. [CrossRef]

236. Sutherland, C. Removal of Heavy Metals from Water using Low-Cost Adsorbents: Process Development. Ph.D. Thesis, The University of the West Indies, Mona, Jamaica, 2004.

237. Hameed, B.H.; El-Khaiary, M.I. Equilibrium, kinetics and mechanism of malachite green adsorption on activated carbon prepared from bamboo by K_2CO_3 activation and subsequent gasification with CO_2. *J. Hazard. Mater.* **2008**, *157*, 344–351. [CrossRef] [PubMed]

238. Zhu, W.; Liu, J.; Li, M. Fundamental Studies of Novel Zwitterionic Hybrid Membranes: Kinetic Model and Mechanism Insights into Strontium Removal. *Sci. World J.* **2014**, *2014*, 1–7. [CrossRef]

239. Vikrant, K.; Kim, K.H.; Ok, Y.S.; Tsang, D.C.W.; Tsang, Y.F.; Giri, B.S.; Singh, R.S. Engineered/designer biochar for the removal of phosphate in water and wastewater. *Sci. Total Environ.* **2018**, *616–617*, 1242–1260. [CrossRef] [PubMed]

240. Milmile, S.N.; Pande, J.V.; Karmakar, S.; Bansiwal, A.; Chakrabarti, T.; Biniwale, R.B. Equilibrium isotherm and kinetic modeling of the adsorption of nitrates by anion exchange Indion NSSR resin. *Desalination* **2011**, *276*, 38–44. [CrossRef]

241. Inyinbor, A.A.; Adekola, F.A.; Olatunji, G.A. Kinetics, isotherms and thermodynamic modeling of liquid phase adsorption of Rhodamine B dye onto Raphia hookerie fruit epicarp. *Water Resour. Ind.* **2016**, *15*, 14–27. [CrossRef]

242. Al-Ghouti, M.A.; Da'ana, D.A. Guidelines for the use and interpretation of adsorption isotherm models: A review. *J. Hazard. Mater.* **2020**, *393*, 122383. [CrossRef]

243. Boni, M.R.; Marzeddu, S.; Tatti, F.; Raboni, M.; Mancini, G.; Luciano, A.; Viotti, P. Experimental and Numerical Study of Biochar Fixed Bed Column for the Adsorption of Arsenic from Aqueous Solutions. *Water* **2021**, *13*, 915. [CrossRef]

244. Langmuir, I. The adsorption of gases on plane surfaces of glass, mica and platinum. *J. Am. Chem. Soc.* **1918**, *40*, 1361–1403. [CrossRef]

245. Jasper, E.E.; Ajibola, V.O.; Onwuka, J.C. Nonlinear regression analysis of the sorption of crystal violet and methylene blue from aqueous solutions onto an agro-waste derived activated carbon. *Appl. Water Sci.* **2020**, *10*, 132. [CrossRef]

246. Freundlich, H.M.F. Über die Adsorption in Lösungen. *Zeitschrift für Phys. Chemie* **1907**, *57*, 385–470. [CrossRef]

247. Halsey, G.D. The role of surface heterogeneity. *Adv. Synth. Catal.* **1952**, *4*, 259–269. [CrossRef]

248. Belhachemi, M.; Addoun, F. Comparative adsorption isotherms and modeling of methylene blue onto activated carbons. *Appl. Water Sci.* **2011**, *1*, 111–117. [CrossRef]

249. Febrianto, J.; Kosasih, A.N.; Sunarso, J.; Ju, Y.H.; Indraswati, N.; Ismadji, S. Equilibrium and kinetic studies in adsorption of heavy metals using biosorbent: A summary of recent studies. *J. Hazard. Mater.* **2009**, *162*, 616–645. [CrossRef]

250. Vilardi, G.; Di Palma, L.; Verdone, N. Heavy metals adsorption by banana peels micro-powder: Equilibrium modeling by non-linear models. *Chinese J. Chem. Eng.* **2018**, *26*, 455–464. [CrossRef]

251. Blahovec, J.; Yanniotis, S. GAB Generalized Equation for Sorption Phenomena. *Food Bioprocess. Technol.* **2008**, *1*, 82–90. [CrossRef]

252. Maroulis, Z.B.; Tsami, E.; Marinos-Kouris, D.; Saravacos, G.D. Application of the GAB model to the moisture sorption isotherms for dried fruits. *J. Food Eng.* **1988**, *7*, 63–78. [CrossRef]

253. Kah, M.; Zhang, X.; Jonker, M.T.O.; Hofmann, T. Measuring and Modeling Adsorption of PAHs to Carbon Nanotubes Over a Six Order of Magnitude Wide Concentration Range. *Environ. Sci. Technol.* **2011**, *45*, 6011–6017. [CrossRef]
254. Terzyk, A.P.; Gauden, P.A.; Kowalczyk, P. What kind of pore size distribution is assumed in the Dubinin–Astakhov adsorption isotherm equation? *Carbon N. Y.* **2002**, *40*, 2879–2886. [CrossRef]
255. Giraldo, J.; Nassar, N.N.; Benjumea, P.; Pereira-Almao, P.; Cortés, F.B. Modeling and Prediction of Asphaltene Adsorption Isotherms Using Polanyi's Modified Theory. *Energy Fuels* **2013**, *27*, 2908–2914. [CrossRef]
256. Sdanghi, G.; Schaefer, S.; Maranzana, G.; Celzard, A.; Fierro, V. Application of the modified Dubinin-Astakhov equation for a better understanding of high-pressure hydrogen adsorption on activated carbons. *Int. J. Hydrogen Energy* **2020**, *45*, 25912–25926. [CrossRef]
257. Brouers, F.; Marquez-Montesino, F. Dubinin isotherms versus the Brouers–Sotolongo family isotherms: A case study. *Adsorpt. Sci. Technol.* **2016**, *34*, 552–564. [CrossRef]
258. Brouers, F.; Al-Musawi, T.J. The use of the Brouers–Sotolongo fractal kinetic equation for the study of drug release. *Adsorption* **2020**, *26*, 843–853. [CrossRef]
259. Wang, J.; Guo, X. Adsorption kinetic models: Physical meanings, applications, and solving methods. *J. Hazard. Mater.* **2020**, *390*, 122156. [CrossRef]
260. Inyang, M.; Dickenson, E. The potential role of biochar in the removal of organic and microbial contaminants from potable and reuse water: A review. *Chemosphere* **2015**, *134*, 232–240. [CrossRef] [PubMed]
261. Oliveira, F.R.; Patel, A.K.; Jaisi, D.P.; Adhikari, S.; Lu, H.; Khanal, S.K. Environmental application of biochar: Current status and perspectives. *Bioresour. Technol.* **2017**, *246*, 110–122. [CrossRef]
262. Krasucka, P.; Pan, B.; Sik Ok, Y.; Mohan, D.; Sarkar, B.; Oleszczuk, P. Engineered biochar—A sustainable solution for the removal of antibiotics from water. *Chem. Eng. J.* **2021**, *405*, 126926. [CrossRef]